

# Recent Progress in Development of Wearable Pressure Sensors Derived from Biological Materials

Hong Pan and Tae-Woo Lee\*

This review summarizes recent progress in the use of biological materials (biomaterials) in wearable pressure sensors. Biomaterials are abundant, sustainable, biocompatible, and biodegradable. Especially, many have sophisticated hierarchical structure and biological characteristics, which are attractive candidates for facile and ecologically-benign fabrication of wearable pressure sensors that are biocompatible, biodegradable, and highly sensitivity. The biomaterials and structures that use them in wearable pressure sensors that exploit sensing mechanisms such as piezoelectric, triboelectric, piezoresistive and capacitive effects are present. Finally, remaining impediments are discussed to use of biomaterials in wearable pressure sensors.

and animals have achieved specialized functions after modification by natural selection over millions of years. Biomaterials have superb biological properties, such as abundant, renewable, biocompatible, biodegradable, self-cleaning, and self-adhesive characteristics. Moreover, many have superb mechanical properties, exceptional topological surface, and intricate hierarchical structures.<sup>[8]</sup> Therefore, these materials may have a wide range of applications in biocompatible, and biodegradable wearable pressure sensors.

Biomaterials provide notable merits and are attractive candidates for environmentally and biologically benign fabrication of wearable pressure sensor.<sup>[9]</sup> These merits

## 1. Introduction

Wearable pressure sensor can mimic the functions of human skin transducing pressure to electronic signals, and therefore have been applied in various fields, including electronic skins (e-skins),<sup>[1]</sup> artificial intelligence,<sup>[2]</sup> soft robotics,<sup>[3]</sup> and human-machine interfacing.<sup>[4]</sup> Importantly, pressure sensors can be mounted on a human body to detect biological signals that are relevant to human health status, so these devices have integral functions in next-generation monitoring systems<sup>[5]</sup> and personal healthcare.<sup>[6]</sup>

Wearable pressure sensors that use biological materials (biomaterials) can be flexible, biocompatible, easy to fabricate, inexpensive, and biodegradable.<sup>[7]</sup> Biomaterials from bacteria, plants,

include: i) abundance and low cost that enable large-scale fabrication of inexpensive devices; ii) exceptional topographic surfaces and intricate structure that provide diverse ways to obtained wearable pressure sensors; iii) diverse functional groups (e.g., hydroxyl, carboxyl, amino) that are easily functionalized; iv) lightweight and biocompatible features to improve the comfort and safety of wearable sensors for long-term and continuous health monitoring; v) biodegradable nature that enables development of implantable devices that break down on a specified schedule, so they need not be removed surgically and avoid the issue of the environmental pollution because of massive electronic waste disposal that will be increased by rapid increase of electronics devices related to the Internet of Things (IoT) and wearable devices. Thus, using of biomaterials will open new possibilities to realize biocompatible, sustainable, low cost, high-performance pressure sensors, especially as implantable sensors.

Herein, we provide an overview of the current status of wearable pressure sensors that use biomaterials (**Figure 1**). The intention is to highlight the importance of utilizing biomaterials for wearable pressure sensors that are biocompatible, biodegradable, and have required sensitivity. Basically, these wearable pressure sensors have been achieved in two ways: by using biologically-inspired structures directly, and by introducing biological materials as components.

Direct use of biological structure has included use of porous,<sup>[10]</sup> and bean pod-like<sup>[11]</sup> structures, and use of natural materials with diverse topographic surfaces<sup>[12]</sup> as soft templates (leaves,<sup>[13]</sup> rose petals<sup>[9a]</sup>) to fabricate structured elastomers. Related uses include use of hierarchically-structure biomaterials<sup>[14]</sup> as skeletons (e.g., cotton cellulose,<sup>[15]</sup> bacterial cellulose<sup>[16]</sup>) to assemble with functional materials to construct flexible structured active materials.

H. Pan, Prof. T.-W. Lee  
Department of Materials Science and Engineering  
Seoul National University  
Seoul 08826, Republic of Korea  
E-mail: twlees@snu.ac.kr

H. Pan  
State Key Laboratory of Electronic Thin Films and Integrated Devices  
School of Optoelectronic Science and Engineering  
University of Electronic Science and Technology of China (UESTC)  
Chengdu 610054, P. R. China

Prof. T.-W. Lee  
School of Chemical and Biological Engineering  
Institute of Engineering Research  
Research Institute of Advanced Materials (RIAM)  
Nano Systems Institute (NSI)  
Seoul 08826, Republic of Korea

 The ORCID identification number(s) for the author(s) of this article can be found under <https://doi.org/10.1002/adhm.202100460>

DOI: 10.1002/adhm.202100460

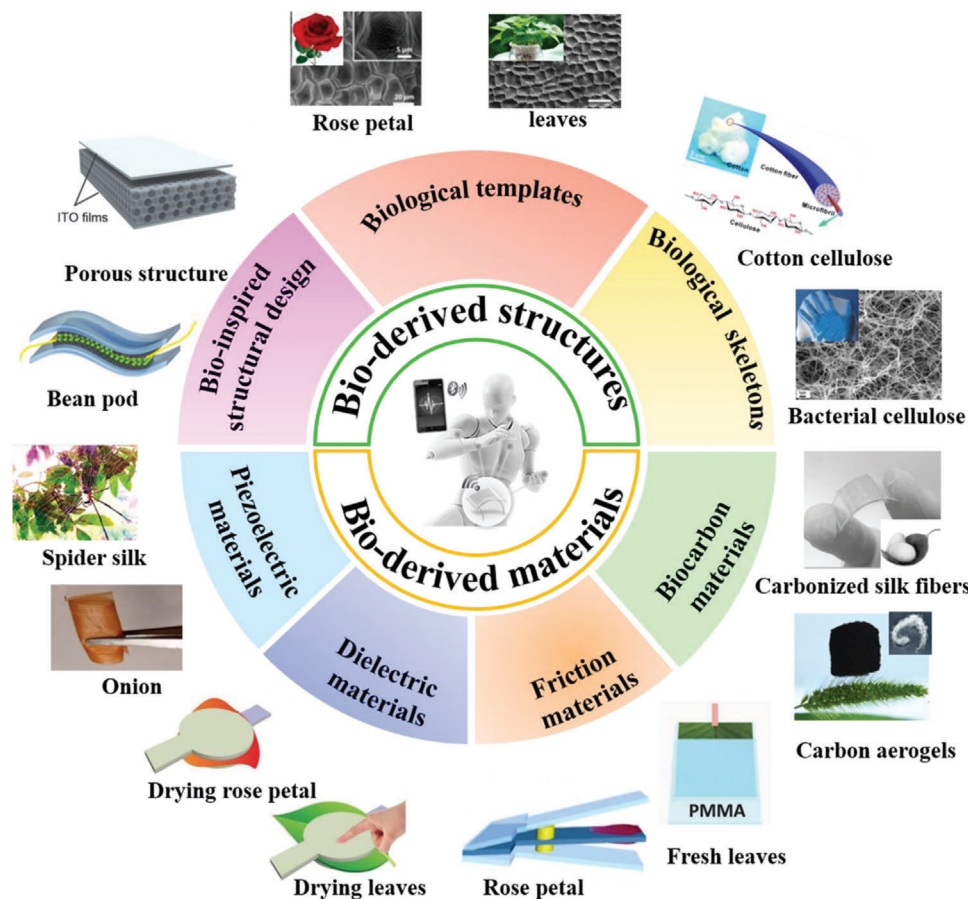


**Figure 1.** Overview of the bioinspired wearable pressure sensors: i) Bioinspired structural design of material and device, such as porous structure and bean pod-like structure. Reproduced with permission.<sup>[10]</sup> Copyright 2016, Wiley-VCH GmbH. Reproduced with permission.<sup>[11]</sup> Copyright 2020, American Chemical Society. ii) biological templates such as rose petals and leaves. Reproduced with permission.<sup>[13]</sup> Copyright 2019, American Chemical Society. Reproduced with permission.<sup>[9a]</sup> Copyright 2020, Wiley-VCH GmbH; iii) biological skeletons, such as cotton cellulose and bacterial cellulose. Reproduced with permission.<sup>[15]</sup> Copyright 2016, The Royal Society of Chemistry. Reproduced with permission.<sup>[16]</sup> Copyright 2015, Wiley-VCH GmbH. And nature-derived materials: i) Biological piezoelectric materials such as spider silk, and onion skin. Reproduced with permission.<sup>[17]</sup> Copyright 2018, Elsevier Ltd. Reproduced with permission.<sup>[18]</sup> Copyright 2017, Elsevier Ltd; ii) biological dielectric materials such as petals and leaves. Reproduced with permission.<sup>[19]</sup> Copyright 2018, Wiley-VCH GmbH; iii) biological friction material such as petals and leaves. Reproduced with permission.<sup>[20]</sup> Copyright 2018, Elsevier Ltd. Reproduced with permission.<sup>[21]</sup> Copyright 2018, Wiley-VCH GmbH; iv) biocarbon materials such as carbonized silk fibers and carbon aerogels. Reproduced with permission.<sup>[22]</sup> Copyright 2017, Wiley-VCH GmbH. Reproduced with permission.<sup>[23]</sup> Copyright 2017, American Chemical Society.

The strategy of introducing biological materials into wearable pressure sensors has exploited biological piezoelectric material such as spider silk<sup>[17]</sup> and onion skin.<sup>[18]</sup> These materials have inherent piezoelectric property without polarization treatment; they can serve directly as active layers in wearable piezoelectric pressure sensors. Biological dielectric materials such as rose petals and leaves<sup>[19]</sup> have diverse surface topographies and intricate microstructure with reversible compressibility and outstanding resiliency, so they are attractive for use in wearable capacitive pressure sensors. Biological friction materials, such as petals<sup>[20]</sup> and leaves,<sup>[21]</sup> have a rough and mechanically flexible surfaces which that can serve as triboelectric materials in wearable triboelectric pressure sensors. Biocarbon materials such as carbonized silk fibers<sup>[22]</sup> and carbon aerogel,<sup>[23]</sup> can serve as conductive material in wearable piezoresistive pressure sensors.

Here, we review the progress in use of using biomaterials in wearable pressure sensors, with particularly focus on structures

and materials derived from biological systems. We first introduce the common sensing mechanisms of the pressure sensors, then present use of biologically-derived structures and materials in wearable pressure sensors. In Section 5, we describe current challenges and suggest future research directions for researchers to fabricate wearable pressure sensors.

## 2. Pressure Sensors and Their Mechanisms

Pressure sensors detect applied pressure or force by converting mechanical stimuli or deformation to assessable electronic signals that can be measured by common electronic equipment. The most common transduction mechanisms of pressure sensors exploit piezoresistive, capacitive, piezoelectric, and triboelectric effects.<sup>[24]</sup> Each of these sensing effects uses a different set of materials and their unique characteristics (Figure 2). Here, we describe these four sensing mechanisms.

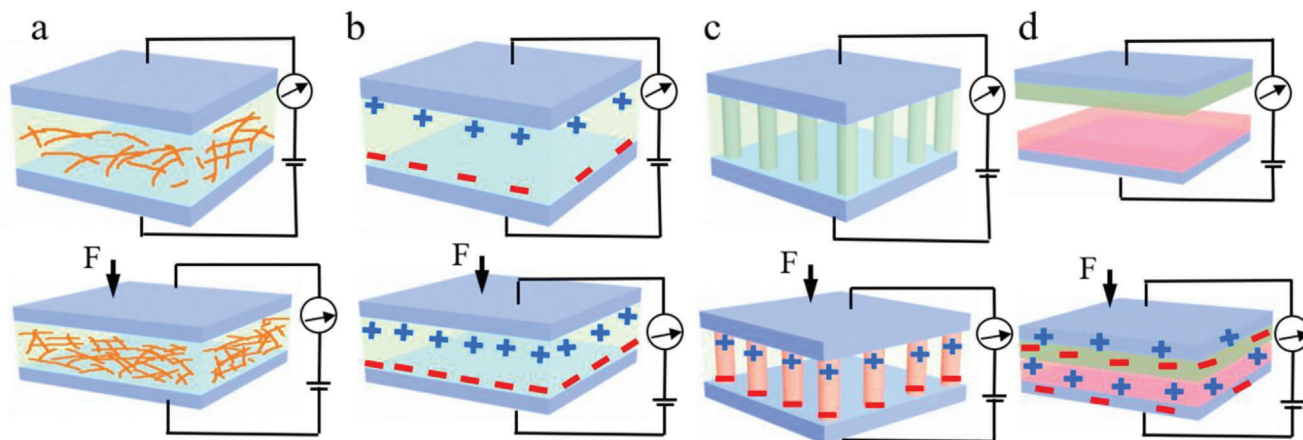


**Figure 2.** Schematic illustrations of four typical transduction mechanisms: a) piezoresistive, b) piezocapacitive, c) piezoelectric, d) triboelectric.

### 2.1. Piezoresistive Effect

Piezoresistive pressure sensors convert applied mechanical stimuli to a change in resistance signal. These pressure sensors generally consist of an elastic conductive or semiconductive sensing material sandwiched between two vertical electrodes or mounted on a pair of parallel interdigitated electrodes (Figure 2a). The resistance  $R$  of materials is calculated as

$$R = \frac{\rho L}{A} \quad (1)$$

where  $\rho$  [ $\Omega$  m] is the material's resistivity,  $L$  [m] is its length, and  $A$  [ $\text{m}^2$ ] is its cross-sectional area. The piezoresistive effect originates from the geometric effect and resistivity effect, as

$$\frac{\Delta R}{R} = (1 + 2\nu)\epsilon + \frac{\Delta\rho}{\rho} \quad (2)$$

where  $\nu$  [dimensionless] is Poisson's ratio and  $\epsilon = \Delta L/L_0$  is the applied strain. The term  $(1 + 2\nu)$  refers to the geometric effect, and  $\Delta\rho/\rho$  refers to the resistivity effect. The geometric effect causes changes in contact resistance, and can be easily tuned by introducing the structural design in devices.<sup>[25]</sup> The resistivity effect derives from changes in band structure<sup>[26]</sup> as well as interparticle distance.<sup>[27]</sup>

Generally, the working principle of piezoresistive pressure sensors that exploit contact resistance is that as pressure is applied, the dimension (such as  $L$ ,  $A$ ) or density of the conductive material changes, so the device's  $\rho$  decreases. These sensors have simple structure, are easy to fabricate, have a simple readout mechanism, and high signal-to-noise ratio (SNR).<sup>[28]</sup> However, they have high power consumption, hysteresis in response, and high drift over time; they also may be sensitive to temperature and humidity, so their applications are constrained.<sup>[1a,25c,29]</sup>

### 2.2. Capacitive Effect

Parallel-plate capacitive pressure sensors are composed of two electrodes separated by an elastomer dielectric layer, which trans-

duces external pressure to a change in capacitance (Figure 2b). The capacitance depends strongly on a geometry effect as

$$C = \frac{\epsilon_0 \epsilon_r A_0}{d} \quad (3)$$

where  $\epsilon_0 = 8.85 \times 10^{-12}$  F m<sup>-1</sup> is the permittivity of vacuum,  $\epsilon_r$  [dimensionless] is the relative permittivity of the dielectric material,  $A_0$  [ $\text{m}^2$ ] is the area of overlap between two electrode parallel plates, and  $d$  [m] is the distance between them.

### 2.3. Piezoelectric Effect

Piezoelectricity refers to the ability of certain materials to generate an electric potential in response to an applied external pressure.<sup>[30]</sup> The phenomenon originates from oriented and permanent dipoles in a material. Piezoelectric pressure sensors generally consist of a piezoelectric material sandwiched between two vertically-aligned electrodes (Figure 2c).<sup>[31]</sup> In general, when an external pressure is applied to the device, the deformation of oriented noncentrosymmetric crystal structures results in spatial separation of positive and negative charges, which leads to formation of charges on the cathode and anode.

Piezoelectric pressure sensors can operate without an external power source for the sensing layer, so they are the most suitable type for dynamic pressure sensing. However, the output signals of these sensors are sensitive to temperature, show high drift in response over time, and interact electrostatically with their surroundings.<sup>[32]</sup>

### 2.4. Triboelectric Effect

A triboelectric pressure sensor transduces a mechanical signal to an electrical signal by coupling contact electrification with electrostatic induction (Figure 2d).<sup>[33]</sup> Periodic contact and separation of two friction materials with different triboelectric polarities generates electrostatic charges, which induce an alternating potential and current. The quantity of electrostatic charges generated highly depends on the difference in triboelectric polarities of

the two friction materials.<sup>[34]</sup> Triboelectric pressure sensors have advantages of low cost, high power density, simple structural design, and no need of external power. By altering the measurement strategy, they can be made to detect both static and dynamic pressure.<sup>[35]</sup>

### 3. Bioderived Structures

Natural selection over millions of years has driven evolution of various biological micro/nanostructures that can help their bearers to survive in complex environment.<sup>[8a,9c,d,12a]</sup> Lotus leaves are superhydrophobic and have a self-cleaning capability due to their rough surfaces with hierarchical microbump structures.<sup>[12b,36]</sup> Spider silk has an excellent combination of strength and elasticity, and is insoluble in water. The orb-shaped spiderweb (consists of several 1D spider silks) is water-repellent and can be used to capture the preys;<sup>[37]</sup> The toes of the Tokay gecko are covered with a skin that has an intricate geometric structure that includes lamellae, setae, branches, and spatula; these structures maximize the skin's adhesive properties, so the gecko can climb vertical surfaces.<sup>[38]</sup> The wide variety of biological structures has offered valuable insights to guide design multiscale structure to improve the flexibility, lifetime, and accuracy of wearable pressure sensor. These structures can be divided into three categories. i) biologically-inspired structural designs, which mimic biological structures to fabricate nature-inspired structural materials and device designs, is expected to endow sensors the extraordinary sensing capabilities; ii) natural templates derive from plant-based materials with diverse topological surfaces and serve as soft templates for lost cost and large-area fabrication of highly sensitive wearable pressure sensors; iii) structural skeletons that originate from biomaterials that consist of intricate fibrous structures and assemble with other functional materials to construct structured sensing material for high-performance devices.

#### 3.1. Bioinspired Structural Design

The diverse environment-adapted structures in nature have endowed living creatures the exceptional sensing capabilities that may guide structural design of material and devices for wearable pressure sensors.<sup>[9c,39]</sup> Bioinspired structural designs, including hierarchical structure,<sup>[40]</sup> porous structure,<sup>[10]</sup> cracked structure,<sup>[41]</sup> interlocked structure,<sup>[42]</sup> bean pod,<sup>[11]</sup> and eardrum,<sup>[43]</sup> have been introduced in wearable pressure sensors to improve their performances and sensing capabilities of a gentle breeze, sound pressure, wrist pulse and the flapping of ladybird. For example, a bioinspired wearable pressure sensor design of hierarchically structured ZnO nanowire (NW) arrays in an interlocked geometry has achieved sensitive detection of static and dynamic pressure stimuli by piezoresistive and piezoelectric transductions (Figure 3a).<sup>[40c]</sup> The implementation of hierarchical structure in an interlocked piezoresistive pressure sensor provides a considerable effective contact area and enables conformal contacts,<sup>[44]</sup> which induce a great change in contact resistance and results in high sensitivity ( $-6.8 \text{ kPa}^{-1}$  at pressure below  $0.3 \text{ kPa}$ ) and low detection limit ( $0.6 \text{ Pa}$ ). Notably, the hierarchical assembly of rigid crystalline ZnO NWs endows these devices

with an ultrafast response ( $\approx 5 \text{ ms}$ ) with minimal hysteresis, so these devices surpass the achievement of conventional pressure sensors that use viscoelastic polymers.<sup>[45]</sup> A Ni film ( $\approx 300 \text{ nm}$ ) coated on one side of interlocked ZnO NW arrays film yielded a piezoelectric pressure sensor, in which the hierarchical design of ZnO NWs enabled instantaneous perception of dynamic stimuli at high frequency vibration ( $250 \text{ Hz}$ ). In comparison with planar structures, the hierarchical NWs provide effective bending of NWs in response to normal pressure, and therefore has increased output current density (Figure 3b) and increased power output  $\approx 5.9 \text{ mW m}^{-2}$ , whereas the planar type had  $\approx 0.5 \text{ mW m}^{-2}$ . The bioinspired multimode wearable pressure sensors have sensing capabilities to monitor static and dynamic tactile perceptions; therefore, these devices are attractive candidates for application in robotic skins and prosthetic limbs.

*Spongia officinalis* is a marine sponge that has a 3D hierarchical structure of pores that have dimensions from nanometers to micrometers. It has high sensitivity, effective deformation, and reversible compressibility, in spite of its light weight and low density.<sup>[46]</sup> These superb mechanical properties of porous structure, such as outstanding flexibility, softness, and resiliency can provide valuable insights to guide structural design of active materials for durable pressure sensors.

A porous PDMS film that was designed to emulate *Spongia officinalis* has been used as an elastic dielectric material to fabricate highly sensitive wearable capacitive pressure sensors.<sup>[10]</sup> The procedure involves three steps: i) coating a PDMS film on polystyrene (PS) latex microbeads that had been uniformly stacked on a Si substrate, ii) etching the PS microbeads in *N,N*-Dimethylformamide to form a porous PDMS film, iii) sandwiching the porous PDMS film between two indium tin oxide (ITO)/polyethylene phthalate (PET) flexible electrodes (Figure 3c). Compared to bare-structured pressure sensor, the porous-structured pressure sensor ( $6 \mu\text{m}$  pore diameter) is seven times more sensitive (Figure 3d). The implement of the porous structures in wearable pressure sensors conspicuously enhanced their sensitivity ( $0.63 \text{ kPa}^{-1}$ ,  $< 1 \text{ kPa}$ ); the change was attributed to two key factors: i) increased elasticity of PDMS dielectric layer, ii) increase in the effective dielectric constant, as a result of the combined effect of PDMS ( $\epsilon_{\text{PDMS}} \approx 3.0$ ) and air in the pores ( $\epsilon_{\text{air}} = 1.0$ ).<sup>[47]</sup> This bioinspired pressure sensor with porous structures had high sensitivity, fast response and relaxation time, a low detection limit ( $2.42 \text{ Pa}$ ), and excellent durability and stability ( $> 10\,000$  cycles). Additionally, this sensor was pixelated into  $15 \times 15$  arrays to enable real-time tactile sensing of various touch shapes.

Bioinspired structural designs of the devices are also crucial to improve the sensitivity and output characteristics of wearable pressure sensors. A capacitive pressure sensor that had a structure that mimicked a bean pod was constructed using a microspacer core layer of elastic polystyrene (PS) microspheres sandwiched between two laser-induced graphene (LIG)/polyurethane (PU) films with 3D porous skeletons.<sup>[11]</sup> The structure was capable of self-healing. The 3D porous-structured LIG pods provide many cavities that can hold PS microspheres beans, and PS microspheres as spacers regulate the extent of physical contact within LIG upon compression, and thereby modulate conductance (Figure 3e).<sup>[48]</sup> In comparison with sensors without any structure mimicking core beans, the introduction of PS microspacer in porous LIG provides numerous conductive

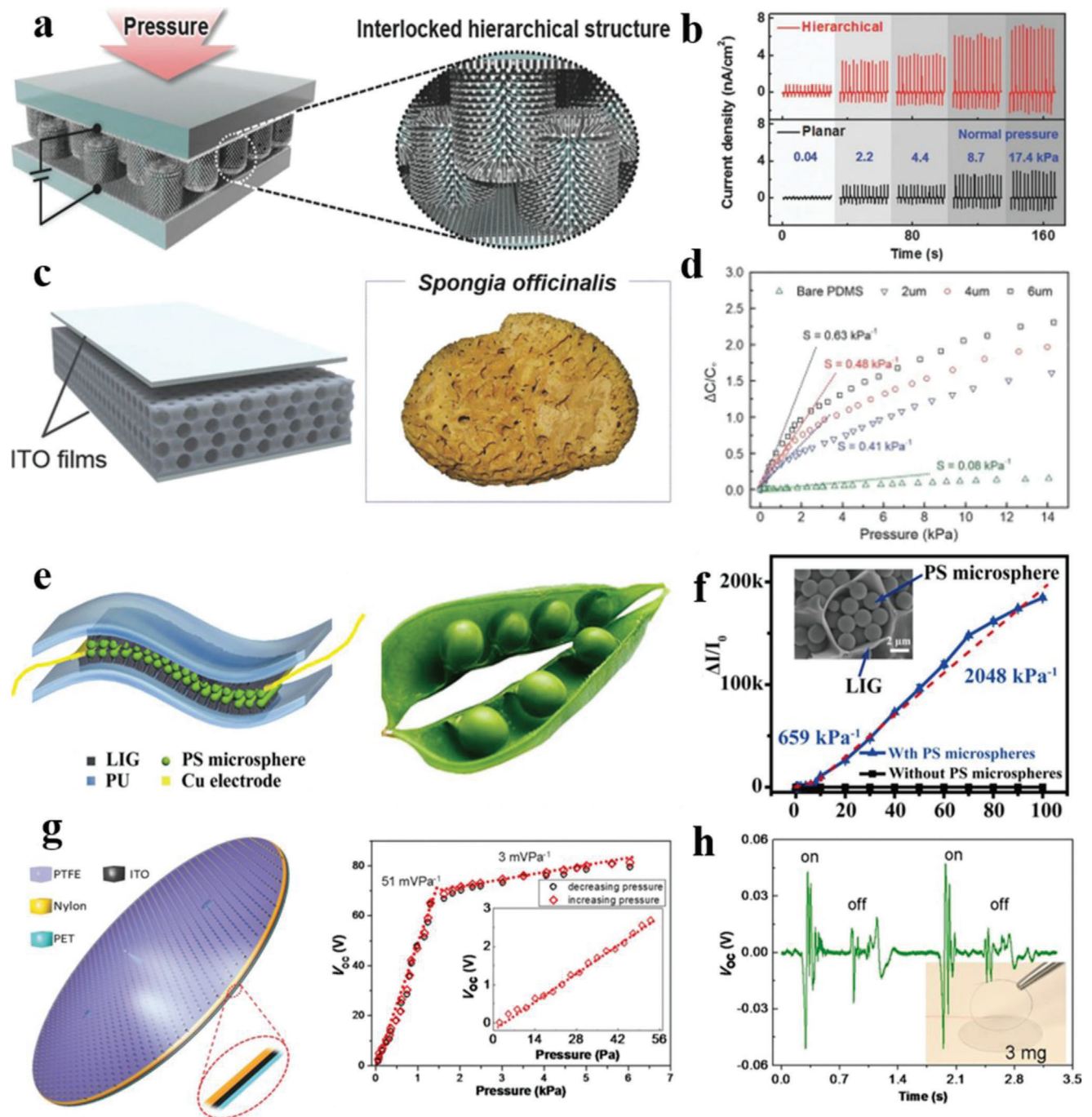


**Figure 3.** Examples of bioinspired structural designs in wearable pressure sensors, including hierarchical structure, porous structure, bean pod, eardrum. a) Schematic illustration of the pressure sensor that uses interlocked geometry of hierarchical ZnO NW arrays. b) Comparison of piezoelectric responses of planar and hierarchical ZnO NW arrays. Reproduced with permission.<sup>[40c]</sup> Copyright 2015, Wiley-VCH GmbH. c) Schematic illustration of wearable pressure sensors based on porous structures, and photograph of a *Spongia officinalis*, d) relative capacitance change to various applied pressures by wearable pressure sensors that exploit porous structure and planar structures. Reproduced with permission.<sup>[10]</sup> Copyright 2016, Wiley-VCH GmbH. e) Schematic illustration of bean-pod-inspired healable wearable pressure sensors and photograph of bean pod, f) response of the wearable pressure sensor with PS microsphere and without PS microsphere. Reproduced with permission.<sup>[11]</sup> Copyright 2020, American Chemical Society. g) Schematic illustration of eardrum-inspired self-powered wearable pressure sensors. h) Electrical and mechanical characterization of the bionic membrane sensor. Reproduced with permission.<sup>[43]</sup> Copyright 2015, Wiley-VCH GmbH.

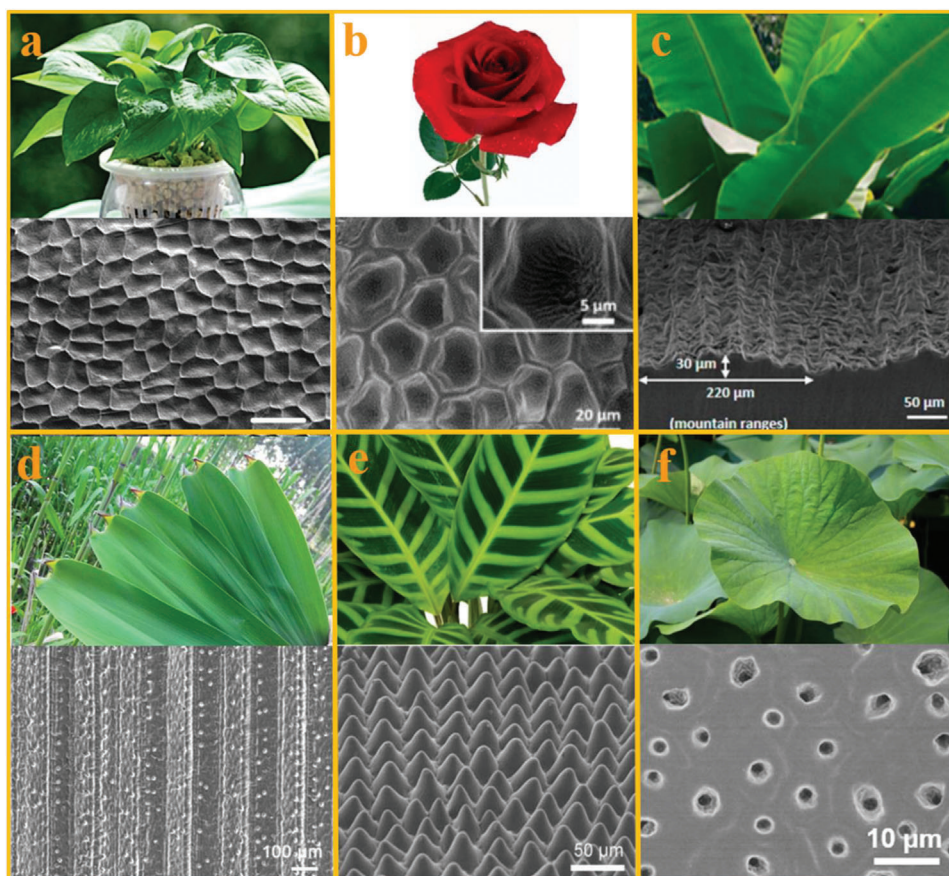


**Figure 4.** Representative photographs of biological materials as soft templates for fabrication of wearable pressure sensors, and scanning electron microscopy (SEM) images of their corresponding microstructural PDMS films. Including: a) *Epipremnum aureum* leaf, Reproduced with permission.<sup>[13]</sup> Copyright 2019, American Chemical Society. b) Rose petal, Reproduced with permission.<sup>[9a]</sup> Copyright 2020, Wiley-VCH GmbH. c) Banana leaf. Reproduced with permission.<sup>[53]</sup> Copyright 2017, American Chemical Society. d) Reed Leaf, Reproduced with permission.<sup>[49]</sup> Copyright 2019, American Chemical Society. e) *Calathea zebrine* leaf, Reproduced with permission.<sup>[50]</sup> Copyright 2018, Wiley-VCH GmbH. f) Lotus Leaf, Reproduced with permission.<sup>[51b]</sup> Copyright 2016, Wiley-VCH GmbH.

paths, and yields wearable pressure sensor that have ultrahigh sensitivity, improved linearity, and a wide sensing range up to 100 kPa. It achieved high sensitivities of 149, 659, and 2048 kPa<sup>-1</sup> for the pressure ranges of 0–1, 1–10, and 10–100 kPa, respectively (Figure 3f). After optimization of both material and structural aspects, this bean pod-inspired pressure sensor is used to monitor a human pulse, and to detect human gait.

Bioinspired structural design has also been implemented in wearable triboelectric pressure sensors. An innovative self-powered bionic membrane sensor (BMS) couples the contact electrification effect with an oval shape inspired by a human eardrum (Figure 3g).<sup>[43]</sup> The BMS is composed of a thin layer of PET film as the bottom supporting substrate, ITO-coated nylon thin film, in which the ITO is the back electrode, the nylon is one electrification layer, and a hierarchical structured polytetrafluoroethylene (PTFE) film is another electrification layer. The three-layered ITO-coated nylon thin film is tented outwards at the level of the tip of an umbo to mimic the human eardrum. The eardrum-inspired structure gives the BMS superior sensitivity in a broad dynamic range (51 mV Pa<sup>-1</sup>, 2.5 Pa–12 kPa), a fast response time < 6 ms, a pressure detection limit down to 2.5 Pa, an excellent cycle stability over 40 000 cycles, and an ul-

trasensitive ability to detect a 3 mg human hair (Figure 3h). The small volume, light weight, low cost, self-powered, and highly-sensitive BMS is an optimal portable sensor for real-time and continuous monitoring of health status by next-generation wearable devices.<sup>[5b]</sup>

### 3.2. Biological Templates

Plant leaves and petals have topological surfaces with abundant biological hierarchical structures, and are candidates as soft templates to help fabricate structured elastomers for highly-sensitive pressure sensors.<sup>[8c,36]</sup> Representatively, *Epipremnum aureum* leaf,<sup>[13]</sup> reed leaf,<sup>[49]</sup> *Calathea zebrine* leaf,<sup>[50]</sup> lotus leaf,<sup>[51]</sup> rose petal,<sup>[9a,52]</sup> and banana leaf<sup>[53]</sup> have been chosen as biological templates for cost-effective and environmentally benign fabrication of micro/nanostructured PDMS film (Figure 4). For example, a highly-sensitive flexible wearable piezoresistive pressure sensor has been constructed using aligned carbon nanotube/graphene (ACNT/G) hybrid films as the active material and microstructured PDMS (m-PDMS) films directly molded from *Epipremnum aureum* leaves as the flexible substrates. As

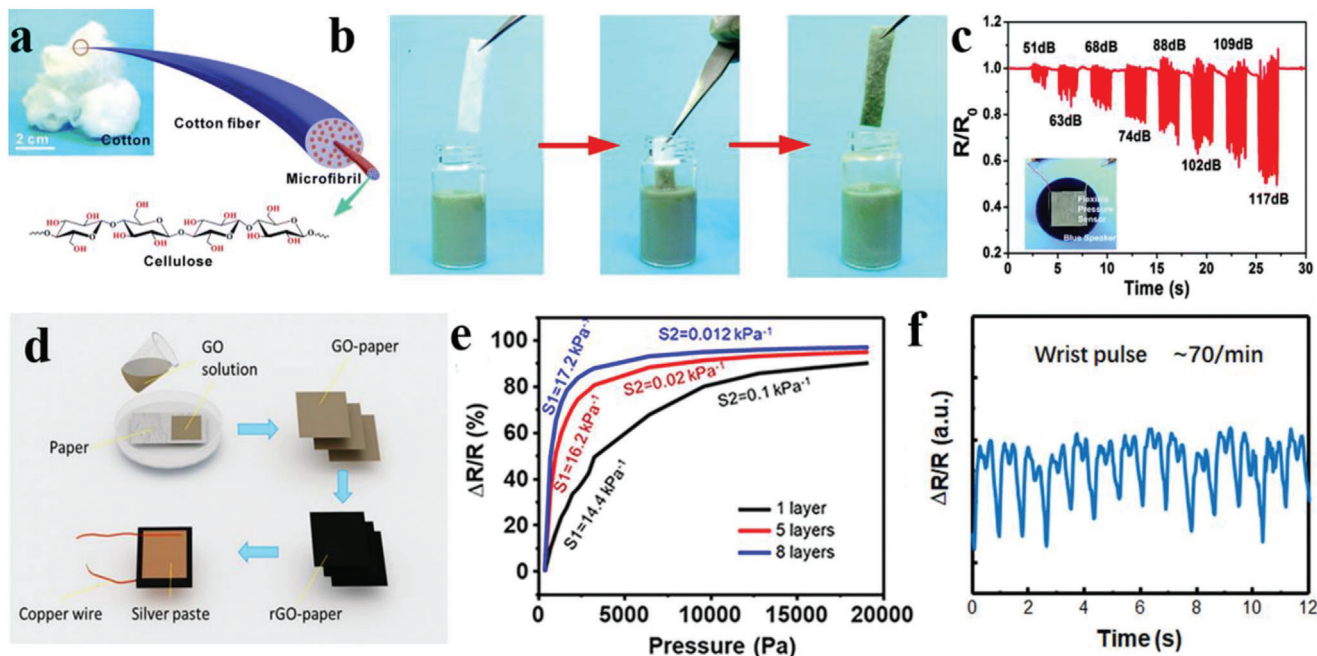


**Figure 5.** Bioderived structures as skeletons in wearable pressure sensors. a) Schematic diagram of the structure of the cotton fibers (inset: optical photograph of natural cotton). b) Fabrication process of cotton/AgNWs sensing material. c) Real-time monitoring of sound-driven vibrations at different sound-pressure levels (SPLs) (inset: flexible pressure sensor attached to Bluetooth speaker). Reproduced with permission.<sup>[15]</sup> Copyright 2016, The Royal Society of Chemistry. d) Fabrication process of pressure sensors that use graphene with paper substrate. e) Change of resistance with pressure increases for sensors that use graphene with one, five, or eight layers of tissue paper. f) Measurement of wrist pulse under normal conditions, indicating 70 beat min<sup>-1</sup>. Reproduced with permission.<sup>[65]</sup> Copyright 2017, American Chemical Society.

a result of a microdome m-PDMS film and ACNT/G with good structural integrity and abundant sensitive sites,<sup>[25b]</sup> the pressure sensor had high sensitivity of 19.8 kPa<sup>-1</sup> (<0.3 kPa), ultralow detection limit of 0.6 Pa, fast response time < 16.7 ms, high durability over 35 000 cycles, and low operating voltage of 0.03 V. Because of these superior traits, these pressure sensors can be applied in numerous applications, such as detection of subtle pressure, bending, torsional forces, and acoustic vibrations.

Hierarchically-structured elastomers, duplicated from biological leaves, can serve as dielectric layers in wearable capacitive pressure sensors. Natural reed leaves have been as soft templates for low-cost and large-area construction of biomimetic micro/nanostructured elastomer for fabrication of sensitive wearable capacitive pressure sensors.<sup>[49]</sup> The capacitive sensor was composed of two thin layers of Au electrodes, one on each side of PDMS (only one side with microgrooves structure). The microgrooves and micropapillae<sup>[54]</sup> gave the capacitive sensor with high sensitivity (0.6 kPa<sup>-1</sup>, in the low-pressure range from 0 to 1 kPa) at low pressure and fast response/recovery time (180/120 ms). These sensors can detect multimodal signals, including tiny forces (e.g., wrist pulses and acoustic vibrations at the throat), and fingers bending. The sensor can also serve as a surface-enhanced Raman scattering (SERS) substrate to detect metabolites in sweat.

The Epidermis of some faunas is composed of hierarchical structures, which are expected to serve as soft templates to fabricate structured elastomer. For example, shark skin is covered by tiny individual tooth-like scales called dermal denticles, ribbed with longitudinal grooves,<sup>[55]</sup> and gecko skin comprises a com-

plex micro- and nanohierarchical structure of lamellae, spatula, setae, and branches.<sup>[8b,56]</sup>

### 3.3. Biological Skeleton

Biological substances, such as cotton,<sup>[57]</sup> collagen aggregates,<sup>[58]</sup> bacterial cellulose,<sup>[59]</sup> and wood<sup>[60]</sup> possess abundant functional groups, high mechanical strength, and fibrous structures, which have been exploited as ideal biological skeletons for low cost and facile construction of structured sensing materials to increase the sensitivity of wearable pressure sensors. For example, wearable piezoresistive pressure sensors that are highly flexible, cost-effective, ecologically benign, and sensitive can be fabricated using porous cotton sheets composed of twisted cotton fibers as a biological network skeleton, combined with silver nanowires (AgNWs) to form a conductive network.<sup>[15]</sup> The surface of cotton bears hydroxyl groups,<sup>[61]</sup> so AgNW conductive networks with high conductivity and durability can be constructed on cotton fiber by using simple dip-coating and subsequent drying (Figure 5a,b). The biobased wearable pressure sensor with high conductivity and durability network structures had high sensitivity (3.4 kPa<sup>-1</sup>, < 100 Pa), rapid response and recovery time (<50 ms) and good stability (> 5000 loading/unloading cycles). Importantly, the pressure sensor can detect and simulate dynamic acoustic vibrations (0.006 dB<sup>-1</sup>), gentle external force, and human body motions (Figure 5c).

Collagen is an abundant, biocompatible, biodegradable, fibrous, and structural protein in all animals, which is an

attractive candidate as natural skeleton to construct structured sensing materials for wearable pressure sensors.<sup>[62]</sup> A collagen aggregate (CA) wearable piezoresistive pressure sensor was fabricated with fibrous CA and polyaniline (PANI)-acidified multiwalled carbon nanotube (H-MWNTs) composites (PANI/H-MWNT, shortly P-M),<sup>[58]</sup> where the CA derived from waste leather were used as the 3D network skeleton and the P-M serve as the conductive materials. The CA sensors have multidimensional recognition ability, which including compressing (gauge factor (GF) = 5.2), bending (GF = 9.2), and twisting strains.

Paper is a recyclable, degradable, flexible, and intrinsic textured fibrous structure,<sup>[63]</sup> and is an attractive candidate as skeleton for wearable pressure sensors that are inexpensive, biocompatible, and biodegradable.<sup>[4a,64]</sup> A reduced graphene oxide-paper (rGO paper) wearable pressure sensor is composed of rGO paper sandwiched between two copper-foil electrodes;<sup>[65]</sup> the rGO paper was obtained by mixing tissue paper with graphene oxide (GO) solution and then be reduced (Figure 5d). With the increase of rGO paper layers, the multilayer pressure sensors developed additional air gaps due to tiny folds on the surface of the paper; they caused rapid decrease in electrical resistance, and thereby increased the sensitivity in the low-pressure range. For the single-layer pressure sensor, the resistance variation mainly relies on the increase in contact area among the inner fibers. Thus, the paper-based pressure sensor with eight layers of rGO papers showed ultrahigh sensitivity of  $17.2 \text{ kPa}^{-1}$  in the wide pressure range 0–20 kPa (Figure 5e). Moreover, this pressure sensor could detect of wrist pulse, speaking, breathing, and motion states (Figure 5f).

Another self-powered paper pressure sensor<sup>[16]</sup> is a piezoelectric wearable pressure sensors that was fabricated using a BaTiO<sub>3</sub> (BTO) /Bacterial cellulose (BC) piezoelectric paper. The piezoelectric paper was obtained using a simple and scalable vacuum-filtration method. The BTO/BC piezoelectric pressure sensors showed outstanding open-circuit voltage output of 14 V and short-circuit current density of  $190 \text{ nA cm}^{-2}$ . Compared with a BTO/PDMS sensor, the introduction of BC in pressure sensor obviously reduced the aggregation of BTO nanoparticles,<sup>[66]</sup> and thereby increased maximum power density by a factor of ten. The flexible BTO/BC piezoelectric pressure sensor is lightweight, ecologically benign, and cheap, so it has possible applications in wearable or implantable energy harvesters and self-powered electronics.

## 4. Bioderived Materials

Biomaterials derived from flora, fauna, bacteria, and viruses have exceptional biological activities and robust hierarchical structures that closely approach perfection through evolutionary adaptation.<sup>[67]</sup> These materials show superb physicochemical and biological properties, and are capable of specialized functions beyond those of synthetic and man-made materials, and therefore have great potential to revolutionize wearable pressure sensor.<sup>[7d,9e]</sup> For example, some biomaterials, such as wood<sup>[68]</sup> and bone<sup>[69]</sup> have piezoelectric properties without polarization treatment. These materials can serve as piezoelectric materials in wearable self-powered pressure sensor and promote the rapid development of portable personal medical monitoring and diagnosis without a need for external power to drive the device.<sup>[70]</sup> Some biomaterials, especially obtained from plants, have plenti-

ful topographic surface<sup>[71]</sup> and intricate innate microstructure<sup>[72]</sup> with reversible compressibility and outstanding resiliency; these traits suggest that the materials can serve as ideal dielectric layers and friction layers without complex treatment in wearable capacitive and triboelectric pressure sensors. Conductive biocarbon materials with unique structures<sup>[73]</sup> have been synthesized from biomaterials by carbonization treatment, and can serve as sensing materials in highly-sensitive wearable piezoresistive pressure sensors. In this section, we overview bioderived materials that provide diverse functions in wearable pressure sensor that exploit the piezoelectric, triboelectric, piezoresistive, or capacitive effect.

### 4.1. Bioderived Piezoelectric Pressure Sensor

The piezoelectric effect in biomaterials was first discovered in collagen-enriched bone structure;<sup>[69]</sup> the discovery provided new insights into biological biomaterials as active layers for biocompatible and wearable piezoelectric pressure sensors. For example, spider silk (SS) is a filamentous protein fiber composed of combination of  $\alpha$ -helix structures alternating with  $\beta$ -sheet crystals, which are strongly interconnected to each other by intra- and intermolecular hydrogen (H) bonds, and develop electrical dipoles inside a lattice crystal. As a benefit of its complex ordered structure, natural SS shows an extraordinary intrinsic piezoelectric property.<sup>[74]</sup> A biopiezoelectric pressure sensors (SSBPPS) has been fabricated using SS after water spraying followed by wrapping;<sup>[17]</sup> the dual water treatments of SS may strongly assist unidirectional alignment of the polymeric chain crystal in SS fibers, and thereby promote efficient polarization (Figure 6a).<sup>[74a,75]</sup> The pressure sensors showed vertical/out-of-plane piezoelectricity ( $d_{zz} \approx 0.36 \text{ pm V}^{-1}$ ) for SS; the result was confirmed using piezoresponse force microscopy analysis. The fabricated SSBPPS has high output voltage ( $\approx 21.3 \text{ V}$ ) and output current ( $\approx 0.68 \text{ }\mu\text{A}$ ) with a maximum instantaneous power density  $\approx 4.56 \text{ }\mu\text{W cm}^{-2}$  and an energy conversion efficiency  $\approx 66\%$  (Figure 6b). This self-powered, biocompatible and ultrasensitive SSBPPS is expected to monitor physiological signals such as arterial pulse, and throat movement during coughing, speaking, or drinking.

Polysaccharides, which mainly exist in plants, can also have piezoelectric characteristics.<sup>[9b,76]</sup> Wood is has piezoelectric properties, but its magnitude is small. The existence of both direct and inverse piezoelectric effects has been proven,<sup>[68a]</sup> and exploited to achieve low shear piezoelectric constant  $d_{14} = 0.1 \text{ pC N}^{-1}$  in the piezoelectric matrix. Wood fiber has its monoclinic regular symmetry and uniaxial cellulose crystal orientation, so electrical dipoles in the crystal structure can be obtained easily.<sup>[77]</sup>

Onion skin (OS) consists of  $\alpha$ -cellulose, carbonyl, carboxyl, and amino groups, as well as N-containing bioligands and quercetin as plant pigment; these components favor intermolecular H-bonding between cellulose molecules and other molecules, and as a consequence yields spontaneous formation of an electric dipole in cellulose microfibrils inside the crystal lattice; therefore, OS is piezoelectric.<sup>[78]</sup> Naturally-abundant self-poled OS has been used as a piezoelectric material ( $d_{14} \approx 2.8 \text{ pC N}^{-1}$ ) to develop a novel biodegradable, biocompatible, inexpensive, and flexible OS biopiezoelectric pressure sensors (OSBPPS) (Figure 6c). The

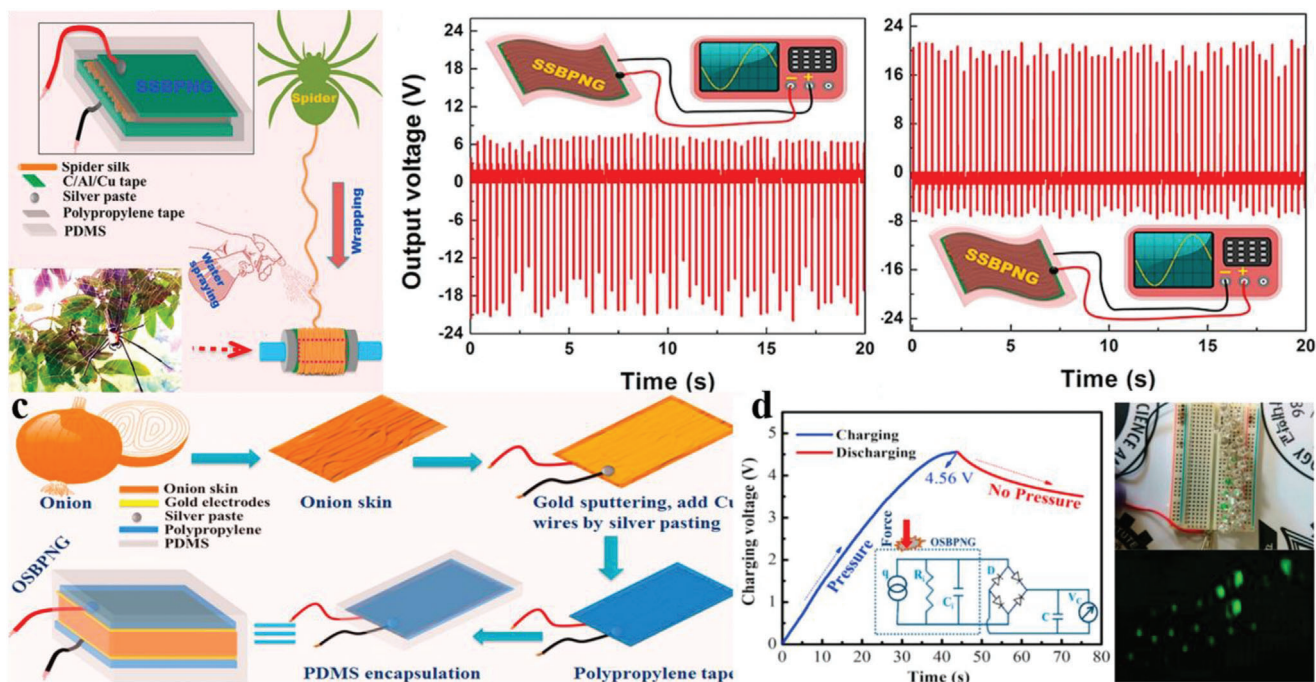


**Figure 6.** a) Schematic of fabrication of spider silk biopiezoelectric pressure sensors (SSBPSS) (inset: photograph of spider with silk web). b) Generated output voltage in forward connection and reverse connection (inset: circuit). Reproduced with permission.<sup>[17]</sup> Copyright 2018, Elsevier Ltd. c) Schematic of fabrication process of onion-skin biopiezoelectric pressure sensors (OSBPSS). d) Charging voltage across a single capacitor ( $4.7 \mu\text{F}$ ) charged by onion skin biopiezoelectric nanogenerator (OSBPNG). e) Power generated from OSBPNG lights up 30 green LEDs instantly (day (top) or night (bottom)). Reproduced with permission.<sup>[18]</sup> Copyright 2017, Elsevier Ltd.

fabricated OSBPSS generated an output voltage of  $\approx 18 \text{ V}$ , current of and  $\approx 166 \text{ nA}$ , instantaneous power density  $\approx 1.7 \mu\text{W cm}^{-2}$  and high piezoelectric energy conversion efficiency  $\approx 61.7\%$ . A single device could instantly turn on 30 green LEDs and power up many other commercial portable electronic displays; it could monitor small strains such as heart beat and throat movement (Figure 6d).

The M13 bacteriophage (phage) is a filamentous bacterial virus composed of single-stranded deoxyribonucleic acid (DNA), which is covered by 2700 copies of a major coat protein (pVIII) and 5–7 copies of two different minor coat proteins (pIII/pVI and pVIII/pIX) located at either end. The pVIII proteins have an  $\alpha$ -helical structure with a dipole moment directed from the amino- to the carboxy-terminal direction and cover the body of the phage with fivefold rotational, twofold screw symmetry, and no inversion center.<sup>[79]</sup> Benefit from its complex structural characteristics, M13 phage show intrinsic piezoelectric properties.<sup>[80]</sup>

Numerous other biomaterials derived from fauna, flora, and viruses have been used in wearable piezoelectric pressure sensor (Table 1). These materials are inherently piezoelectric without any further chemical treatment, so they serve as self-poled piezoelectric materials for cost-effective and ecologically-benign fabrication of wearable self-powered devices for personal monitoring, such as wrist pulse, throat movement, and motion states.

#### 4.2. Bioderived Triboelectric Pressure Sensors

Biomaterials can be exploited in biocompatible triboelectric pressure sensors to meet the demand for portable personal medical

monitoring.<sup>[92]</sup> The surfaces of these materials have hierarchical-structure, which provide a sophisticated friction surface, enlarge the contact area between friction materials and improve the output characteristics;<sup>[93]</sup> and can be used as templates for surface modification of polymers by soft lithography.<sup>[94]</sup> These traits have been exploited<sup>[95]</sup> to develop a biotriboelectric pressure sensor (BTPS) (Figure 7a) that using bacterial nanocellulose (BNC) as a friction material, copper (Cu) foil on the upper side as a current collector, and a layer on the lower side that serves as both current collector and friction material. The relationship between power generation and the structural aspects, including the curvature and friction area, was investigated in view of optimization. This device provides new insights to methods to develop biocompatible and ecologically-benign triboelectric pressure sensors and optimization strategies to realize highly sensitive devices.

Triboelectrification occurs naturally in many plants. The phenomenon on fresh rose petals has been exploited to fabricate a petal-triboelectric pressure sensor (petal-TPS)<sup>[20]</sup> (Figure 7b), in which the top and bottom poly (methyl methacrylate) (PMMA) provide substrates to provide stimulation or stress, rose petals are attached on the surface of middle PMMA, and a spacer establishes appropriate spacing to improving the efficiency of vibration. Comparative experiments verified that the triboelectrification on a rose petal could generate electricity by coupling of the electric static effect, with the petal tissue mainly acting as an electrical conductor. The rich micro/nanostructures on the petal surface provided sufficient roughness for hydrophobicity, and sufficient contact area to maximize triboelectrification,<sup>[96]</sup> so

**Table 1.** Output characteristics of typical bioderived piezoelectric pressure sensors.

| Natural origin | Material used in PNG  | Output voltage;<br>current [V; $\mu$ A] | Energy conversion<br>efficiency [%] | Piezoelectric<br>coefficient [ $\text{pC N}^{-1}$ ] | Power density [ $\mu\text{W cm}^{-2}$ ] | Ref.  |
|----------------|-----------------------|---|-------------------------------------|---|---|-------|
| Fauna          | Spider silk           | 21.3; 0.68                              | 66                                  | 0.36  | 4.56                                    | [17]  |
|                | Fish scale            | 4; 1.5                                  | 46.7                                | 5   | 1.14                                    | [81]  |
|                | Fish skin             | 2; 20                                   | 1.3                                 | 3   | 750                                     | [82]  |
|                | Fish swim bladder     | 10; 51                                  | 0.3                                 | 22  | 4.15                                    | [83]  |
|                | Crab shell            | 22; 1.2                                 | — <sup>a)</sup>                     | 9.49  | 97                                      | [84]  |
|                | Human bone            | —; —                                    | —                                   | 0.22  | —                                       | [85]  |
|                | Dental tissue         | —; —                                    | —                                   | 0.027   | —                                       | [85]  |
|                | Eggshell              | 26.4; 1.45                              | 63                                  | 23.7  | 238.17                                  | [86]  |
|                | Prawn shell           | 4.4; 0.0037                             | 38                                  | −2  | 0.76                                    | [87]  |
| Flora          | Onion                 | 18; 0.166                               | 61.7                                | 2.8   | 1.7                                     | [18]  |
|                | Aloe vera             | 1.2; 0.2                                | —                                   | 6.5   | —                                       | [88]  |
|                | Orange peel           | 30; —                                   | —                                   | —   | 25                                      | [89]  |
|                | Pomelo fruit          | 6.4; 7.44                               | 75                                  | —   | 12                                      | [90]  |
| Virus          | M13 phages            | 0.4; 0.006                              | —                                   | 7.8   | —                                       | [80a] |
|                | M13 phage nanopillars | 0.14; 0.0095                            | —                                   | 10  | $8.7 \times 10^{-5}$                    | [91]  |

<sup>a)</sup> “—” means not stated.

the petal-TPS could monitor the falling process of water droplets without external power.

A fresh leaf contains abundant water and electrolytes, which can be used as a conductive liquid in leaf-triboelectric pressure sensor (leaf-TPS),<sup>[21]</sup> (Figure 7c) in which a fresh leaf from *Hosta plantaginea* provides both a friction layer and an electrode, a metal electrode is connected to the leaf to provide an electrical path, and a polymer sheet with significant difference in electron affinity than the leaf surface is chosen as the contact layer. Use of various species of leaves that have different surface electron affinity in the leaf-TPS can yield significant differences in electric output (Figure 7d). These plant-TPS have potential applications in the IoT and self-powered systems.

Fresh leaves dry out, so a leaf-TPS that uses fresh leaves was compared to one that uses dry leaves (Figure 7e).<sup>[97]</sup> Compared with TPS based on the dry leaf, the TPS that used the fresh leaf had lower electric output, mainly because the free water in the fresh leaf reduced the generation of electrons (Figure 7f). To overcome the fragility of the dry leaf, it was milled to leaf powder to overcome the problem that the leaf cannot directly serve integral friction. The as-fabricated TPS that uses leaf powder had a little higher output than the dry leaf due to its flat surface and microparticulate structures. To further improve the output characteristics of the TPS that uses leaf powder, poly-L-Lysine (PLL) was used to modify the powder's surface; this treatment increased the output current the TPS to as high as 60  $\mu$ A, and its output voltage to as much as 1000 V, which are more than double the values of the unmodified leaf powder.

Silk fibroin (SF) is a mechanically strong, superior electronegativity and fibrous structure biomaterial,<sup>[7c]</sup> which can be served as superb friction layer to fabricate triboelectric pressure sensor. A silk fibroin nanofiber-networked biotriboelectric pressure sensor (SF-BTPS)<sup>[98]</sup> is composed of two arch-shaped friction layers (an electrospun silk fibroin nanofiber film and a PI film) and a cur-

rent collector (Al foil). As a benefit of the nanofibrous silk fibroin film with ultrahigh surface-to-volume ratio and much rougher surfaces than bare film, the peak-voltage of the electrospun SF-BTPS was about 1.5 times higher than that of the cast SF-BTPS. The triboelectric surface charge density and the instantaneous electric power of the electrospun SF-BTEG were measured up to 1.86  $\mu\text{C m}^{-2}$  and 4.3  $\text{mW m}^{-2}$ , respectively. Most interestingly, the SF-BTEG shows exceptionally durable and reliable energy harvesting performances, which has great potential for self-powered systems even under environments of harsh vibration and in living organisms with no harmful effects.

### 4.3. Bioderived Piezoresistive Pressure Sensor

Some biomaterials have complex inner hierarchical architecture, such as the fibrous structures of silkworm silk,<sup>[7c,66a]</sup> spider silk,<sup>[74b,75]</sup> cotton,<sup>[15,99]</sup> bacterial cellulose,<sup>[100]</sup> animal collagen,<sup>[58]</sup> the tubular structures of poplar catkins,<sup>[23]</sup> the honeycomb and foam microstructures of wood,<sup>[101]</sup> and hollow structures of sunflower pollen.<sup>[102]</sup> These materials are attractive candidates for low-cost and facile preparation of conductive structured biocarbon materials to fabricate highly-sensitive wearable piezoresistive pressure sensors. For example, skin-like wearable piezoresistive pressure sensors have been fabricated using carbonized silk nanofiber membranes (CSilkNM) as the active materials and planar PDMS films as the flexible substrates (Figure 8a).<sup>[22]</sup> CSilkNM with good transparency and excellent flexibility could be obtained from silkworm silk by electrospinning and carbonization, then integrated with planar PDMS films to fabricate a wearable sensor without needing complex microengineering treatment. The CSilkNM pressure sensors had high sensitivity (34.47  $\text{kPa}^{-1}$ , pressure range of 0.8–400 Pa), ultralow detection limit (0.8 Pa), fast response time (<16.7 ms), and high stability

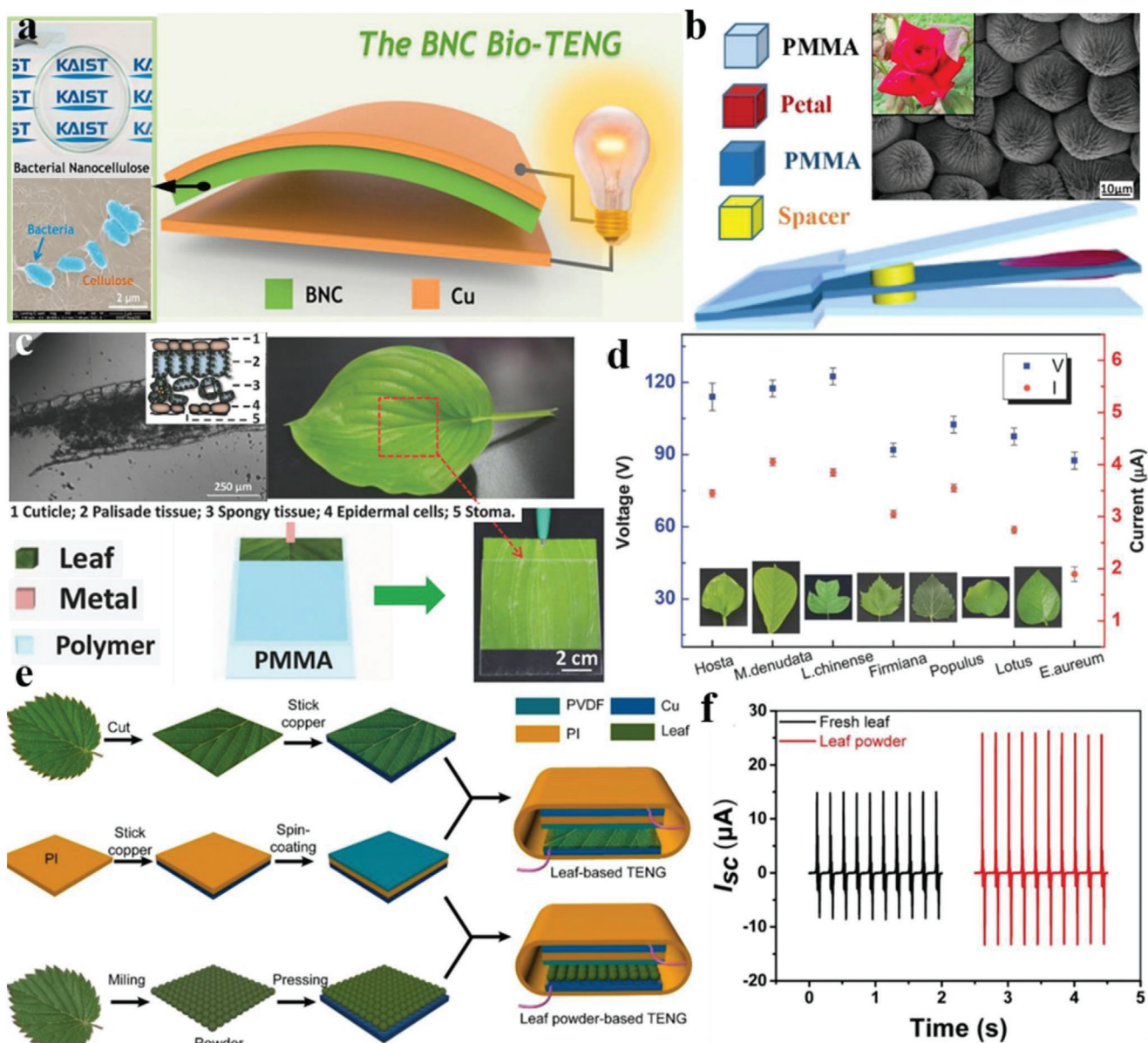


**Figure 7.** Typical bio-derived wearable triboelectric pressure sensors (WTPS). a) Demonstration of a BNC-based TPS. Reproduced with permission.<sup>[95]</sup> Copyright 2017, Elsevier Ltd. b) Schematic diagram of the WTPS that use rose petals (inset: SEM image of rose petal). Reproduced with permission.<sup>[20]</sup> Copyright 2018, Elsevier Ltd. c) Structure of natural-leaf-assembled WTPS in single-electrode mode (inset: photomicrograph of cross section of the Hosta leaf). d) Electrical output of leaf-TPS (PMMA) assembled with various leaves (insets: photograph of corresponding leaf). Reproduced with permission.<sup>[21]</sup> Copyright 2018, Wiley-VCH GmbH. e) Schematic illustration of fabrication process of leaf and leaf-powder WTPS. f) Short-circuit current of the fresh-leaf and leaf-powder WTPS. Reproduced with permission.<sup>[97]</sup> Copyright 2018, Elsevier Ltd.

(>10 000 cycles). These CSilkNM pressure sensors can monitor human physiological signals, such as wrist pulses, respirations, and deep jugular venous pulses (Figure 8b).

Silk fibroin (SF) has abundant functional groups (NH-, OH-), which can serve as a bridging agent to self-assemble pristine  $\text{Ti}_3\text{C}_2\text{T}_x$  MXene nanosheets into a continuous wave-shaped lamellar macrostructure.<sup>[103]</sup> The SF/MXene biocomposite films with 3D cross-link structure exhibits good mechanical and pressure-sensing performance, including low elastic modulus

(1.22 MPa), good sensitivity ( $25.5 \text{ kPa}^{-1}$ , in the low-pressure ranges from 100 to 500 Pa), relatively short response/recovery time (40/35 ms), and low detection limit (9.8 Pa). Because of its superior sensing performance, the SF/MXene pressure sensor can detect minuscule deformations of the human body, such as phonations and wrist pulses.

Biocarbon materials derived from plant materials that have fibrous,<sup>[104]</sup> tubular,<sup>[23]</sup> or hollow<sup>[105]</sup> structure have been widely applied in wearable piezoresistive pressure sensor. Sunflower

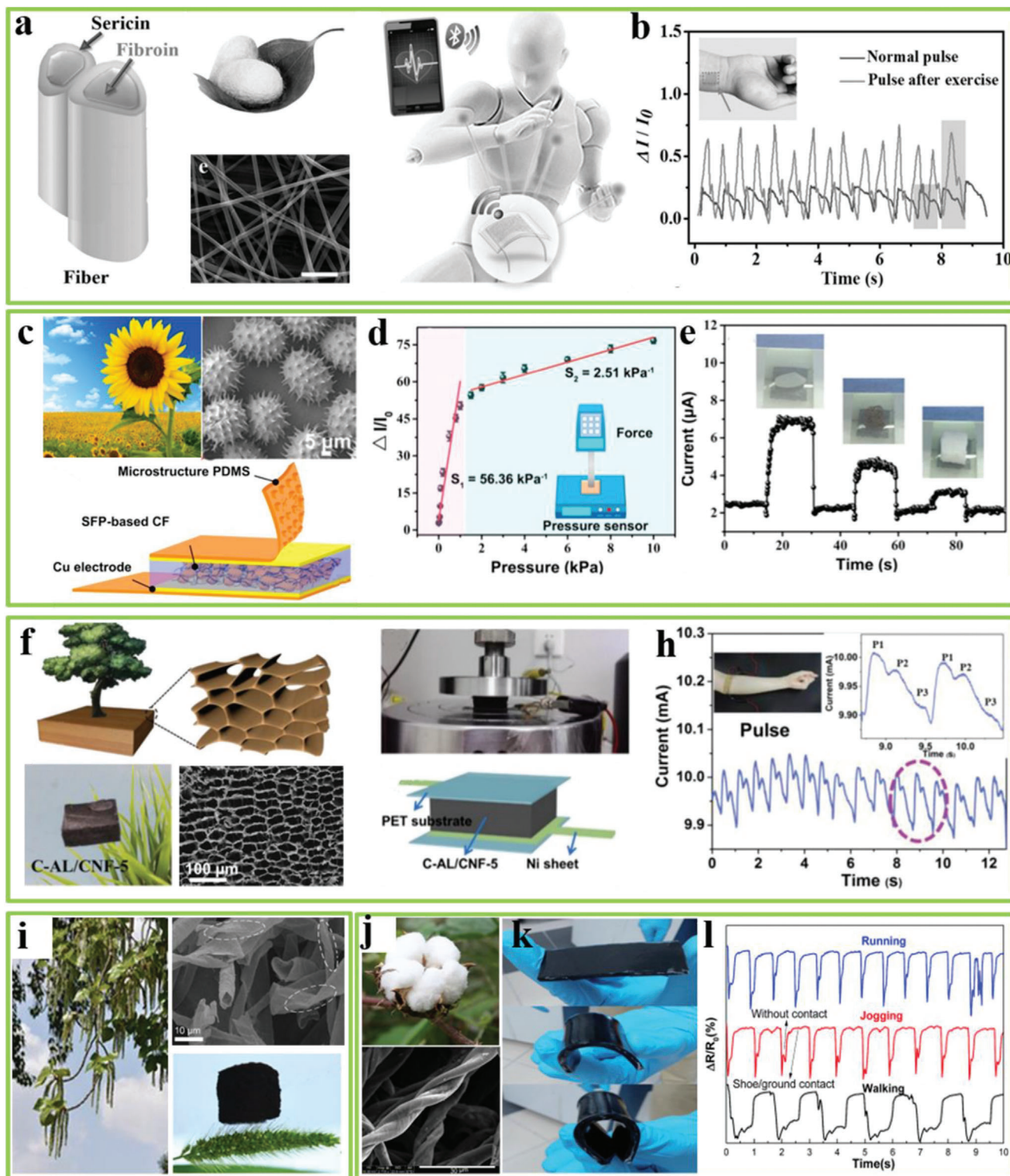


**Figure 8.** Typical biocarbon derived from biological materials in wearable piezoresistive pressure sensor (WRPS): WRPS that uses carbonized silkworm silk (CSWS). a) Schematic diagram of CSWS WRPS (inset: SEM image of CSWS). Scale bar: 1  $\mu\text{m}$ . b) Real-time monitoring of human wrist pulses under normal condition and exercise condition (inset: photograph of the pressure sensors attached to a human wrist). Reproduced with permission.<sup>[22]</sup> Copyright 2017, Wiley-VCH GmbH. WRPS that uses carbonized seed of sunflower (CSSF). c) Schematic diagram of the WRPS that uses CSSF, optical image of the sunflower plant and SEM image of the sunflower pollen. d) Sensitivity of CSSF WRPS. e) Transient response of the pressure sensor to loading and removal of rice grain (25 mg), copper wire (15 mg), and foam (4 mg); the weight of foam corresponded to a pressure of only 1.6 Pa. Reproduced with permission.<sup>[102]</sup> Copyright 2017, Elsevier Ltd. WRPS that uses wood-derived carbon aerogel. f) Schematic diagram of wood-derived

pollen (SFP) has been used as hollow microcapsules as the active component to fabricate a highly sensitive pressure sensor.<sup>[102]</sup> To increase enhance the sensing capabilities, the hollow microcapsules were functionalized with carbon nanotubes, then encapsulated in microstructured PDMS film (Figure 8c). The devices had high sensitivity ( $56.36 \text{ kPa}^{-1}$ , at low pressure 0–1 kPa), excellent stability ( $>25\,000$  cycles), and low detection limit (1.6 Pa) (Figure 8d,e). Importantly, the use of pollen as microcapsules enabled waterproofing for highly stable operation under varying humidity conditions, so all-weather use is possible.

Carbon aerogels are chemically inert, and have low density, high porosity, high conductivity, and interconnected 3D network structure;<sup>[106]</sup> therefore, they are superb sensing materials for highly-sensitive piezoelectric pressure sensors. A wood-derived lightweight carbon aerogel with ordered tracheid-like texture has been fabricated<sup>[101]</sup> by directional freezing-casting, vacuum freeze-drying, and carbonization of wood-derived cellulose nanofibers (CNFs) and alkali lignin (AL) (Figure 8f). Lignin has high thermal stability and weight retention after annealing, so the introduction of lignin successfully restricted severe crimping of CNFs and effectively reduced the severe volume shrinkage of the aerogel network, and hence minimized the structural damage and led to ordered tracheid-like structure. This structure in the wood-derived carbon aerogel gave it excellent mechanical characteristics, including high compressibility (up to 95% strain), good elasticity, and excellent fatigue resistance. As a result of these merits, the CNF wearable pressure sensors had high sensitivity at a wide working pressure range of 0–16.89 kPa, and could accurately detect physiological signals (Figure 8h).

Carbon aerogel with special hollow 3D networks has been synthesized by simple heat treatment and freeze drying of poplar catkin (PC) fibers, which have a tubular structure.<sup>[23]</sup> This process requires sodium chlorite (SC) treatment. The as-fabricated carbon aerogel had ultralow density ( $4.3 \text{ mg cm}^{-3}$ ), high compressibility (80%), high electrical conductivity ( $0.47 \text{ S cm}^{-1}$ ), and high absorbency ( $80\text{--}161 \text{ g g}^{-1}$ ) for oils and organic liquids. As a result of its excellent mechanical properties and electrical conductivity, carbon aerogel with tubular structure is a superb elastomeric conductor.

Cotton is composed of 90–95% cellulose, and is a useful raw material for fabrication of porous carbon. Pyrolysis of fluffy cotton yields a sponge-like carbon cotton (CC) (Figure 8j),<sup>[104b]</sup> which has moderate electrical conductivity ( $11 \text{ S m}^{-1}$ ) as a result of its interconnected carbon fiber networks. CC is highly porous, so the flexible and conductive CC/PDMS composites were fabricated by vacuum-assisted infusion of PDMS resin into a CC scaffold (Figure 8k). Wearable pressure sensors that use CC/PMDS composites showed good sensitivity in a wide range of working pressure up to 700 kPa, a wide response frequency from 0.01 to 5 Hz, and a high durability over 1000 cycles. The device can be fixed on a sport shoe or waist belt to monitor motion state and health condition (Figure 8h).

#### 4.4. Bioderived Capacitive Pressure Sensor

Plant leaves and petals show reversible compressibility, soft bendability, and outstanding resiliency due to innate microstructure that composed of a 3D cell-wall network,<sup>[12c,107]</sup> which can serve as splendid dielectric materials in capacitive pressure sensors. This biological material has been used as a dielectric layer to fabricate a simple and low-cost wearable capacitive pressure sensor (Figure 9a).<sup>[19]</sup> The biological material was treated using critical point drying, which removed the water from the material to improve its stability while retaining the surface morphology and inner structures. As a consequence of surface microstructure and foam-like hollow structure of the dried rose petal, devices that used it had a high sensitivity of  $1.54 \text{ kPa}^{-1}$  at low pressure ( $<1 \text{ kPa}$ ), and exceptional stability over 5000 cyclic loading/unloading or 5000 cyclic bends to a radius of 3 mm (Figure 9b–e). These sensors have been applied to sense touch, monitor motion, detect gas flow, and monitor the spatial distribution of pressure (Figure 9h).

A capacitive pressure sensor has been fabricated using plant-derived materials.<sup>[108]</sup> A leaf skeleton coated with Ag NWs was used as a breathable and flexible electrode, and a rose petal was used as the dielectric layer. The leaf skeleton had a network-like structure, and the electrode has transparency of 60–75% at wavelengths 400–900 nm. The leaf skeleton has a rough fractal-like architecture that offers good adhesion to Ag NWs, and maintains interconnection between the Ag NWs when the electrodes are bent. The sensor has been used to sense touch and to monitor gestures.

## 5. Conclusion and Perspective

Biomaterials are abundant, sustainable, biocompatible, and biodegradable. Many have intricate hierarchical structures and exceptional biological activities. Therefore, biomaterials are attractive candidates for cheap and ecologically-benign fabrication of conformal next-generation wearable pressure sensors that are biocompatible, biodegradable, and highly sensitivity. In this review, we introduced recent advances in the use of biomaterials for wearable pressure sensors, and discussed the advantages of bioderived structures and bioderived materials in wearable pressure sensors.

Notably, the environment-adapted structures in nature have endowed living creatures with exceptional sensing capabilities, which provide valuable and novel insights for structural designs of materials and devices for highly-sensitive wearable pressure sensors. These bioinspired structural designs, including hierarchical structure, porous structure, interlocked structure, bean pod, and eardrum, endow wearable pressure sensors with remarkable sensing capabilities. Moreover, biomaterials can have complex topographical surfaces that can serve as soft templates for low-cost and large-area fabrication of structured elastomers

---

carbon aerogel alkali lignin (C-AL)/CNF. h) Real-time monitoring of arm pulse (inset: photograph of the pressure sensor attached to a human arm). Reproduced with permission.<sup>[101]</sup> Copyright 2020, Wiley-VCH GmbH. i) WRPS that uses carbon aerogels derived from Poplar catkin (PC) fibers, and SEM image of carbonized PC carbon aerogels. Reproduced with permission.<sup>[23]</sup> Copyright 2017, American Chemical Society. The WRPS that uses carbonized cotton. j) Photograph of natural cotton and SEM image of carbonized cotton fiber. k) Photograph of WRPS that uses carbonized cotton. l) Real-time detection of different human movements. Reproduced with permission.<sup>[104b]</sup> Copyright 2015, The Royal Society of Chemistry.

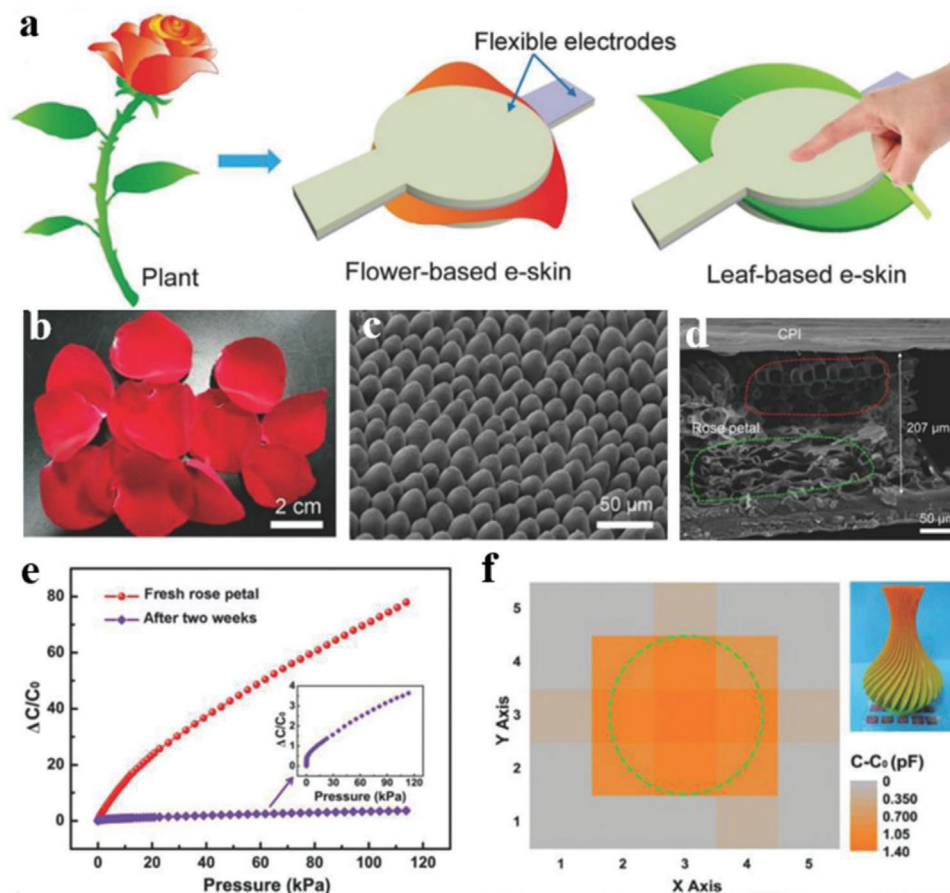


**Figure 9.** Natural plant material as dielectric layers in wearable capacitive pressure sensor (WCPS). a) Schematic illustration of the e-skin consisting of two electrodes, separated by biological material as the dielectric layer. b) Photograph of red rose petal. c) A 45°-tilted view SEM image of rose petal after critical-point drying. d) Cross-sectional SEM image of pressure sensors that uses biological material. e)  $\Delta C/C_0$  as a function of pressure of the e-skins that use a fresh petal and the property after 2 weeks. f) Pressure-distribution mapping by sensor array when a vase is placed on it. All panels reproduced with permission.<sup>[19]</sup> Copyright 2018, Wiley-VCH GmbH.

for highly sensitive wearable pressure sensors. Biomaterials (e.g., cotton, wood, bacterial cellulose) also possess abundant functional groups, excellent mechanical strength and inner micro/nanostructures, which can serve as natural skeletons and be assembled with functional materials (e.g., MXene, CNT, GO, and BaTiO<sub>3</sub>) to construct structured sensing materials for wearable pressure sensors.

Biomaterials also have superb physicochemical and biological properties, and are capable of specialized functions beyond those achievable by synthetic materials, and therefore which can serve as exceptional active materials in wearable pressure sensors that exploit piezoelectric, triboelectric, piezoresistive, or capacitive effects. Some biomaterials (e.g., spider silk, fish skin, onion, and fruit peel) have an inherent piezoelectric property, which can be used directly in wearable piezoelectric pressure sensors without polarization treatment. Leaves and petals have a topographically-complex surfaces and intricate inner microstructure with reversible compressibility and outstanding resiliency, so they can serve as ideal dielectric layers and friction layers without complex treatment, and can be used in wearable capacitive or triboelectric pressure sensors. Conductive biocarbon ma-

terials that have fibrous structures, tubular structures, hollow structure, and cellular structures provide attractive components for use in fabrication of highly sensitive wearable piezoresistive pressure sensors.

Before wearable pressure sensor can be used in realistic applications, several limitations must be overcome. First, biomaterials have relatively low piezoelectric coefficients, so improvement of sensing capability is still a challenge for wearable piezoelectric pressure sensors. Second, the mechanical flexibility and electrical conductivity of biocarbon materials after carbonization treatment must be improved, to increase the conformability and sensing sensitivity of wearable piezoresistive pressure sensors. Third, structured elastomers that are fabricated by replication of leaves or petals, are usually irregular and have low porosity and poor repeatability. Fourth, the structure–property relationships between biomaterials and wearable pressure sensors should be clarified, then used to guide development of methods to increase the sensitivity of sensors. Fifth, the practical portable application requires wireless data transmission to a Bluetooth enabled smartphone for analysis or even sending the data to cloud servers. Finally, devices with fresh biomaterials may dry out over time, and thus lose

their sensing capacities. Although challenges remain, biomaterials have great potential for use in next-generation wearable pressure sensors.

## Acknowledgements

This work was supported by the National Research Foundation of Korea (NRF) grant funded by the Korea government (MSIT) (No. NRF-2016R1A3B1908431). This research was also supported by Creative-Pioneering Researchers Program through Seoul National University (SNU).

## Conflict of Interest

The authors declare no conflict of interest.

## Keywords

biological materials, hierarchical structures, pressure sensors, wearable devices

Received: March 10, 2021

Revised: April 17, 2021

Published online:

- [1] a) Z. Lou, S. Chen, L. Wang, R. Shi, L. Li, K. Jiang, D. Chen, G. Shen, *Nano Energy* **2017**, *38*, 28; b) P. Tan, Y. Zou, Y. Fan, Z. Li, *Wearable Technol.* **2020**, *1*, e5.
- [2] Y. Zang, F. Zhang, C.-a. Di, D. Zhu, *Mater. Horiz.* **2015**, *2*, 140.
- [3] Y. Kim, A. Chortos, W. Xu, Y. Liu, J. Y. Oh, D. Son, J. Kang, A. M. Foudeh, C. Zhu, Y. Lee, S. Niu, J. Liu, R. Pfattner, Z. Bao, T.-W. Lee, *Science* **2018**, *360*, 998.
- [4] a) Y. Guo, M. Zhong, Z. Fang, P. Wan, G. Yu, *Nano Lett.* **2019**, *19*, 1143; b) X. Wu, Y. Han, X. Zhang, Z. Zhou, C. Lu, *Adv. Funct. Mater.* **2016**, *26*, 6246.
- [5] a) C. M. Boutry, A. Nguyen, Q. O. Lawal, A. Chortos, S. Rondeau-Gagne, Z. Bao, *Adv. Mater.* **2015**, *27*, 6954; b) Z. Liu, Y. Ma, H. Ouyang, B. Shi, N. Li, D. Jiang, F. Xie, D. Qu, Y. Zou, Y. Huang, H. Li, C. Zhao, P. Tan, M. Yu, Y. Fan, H. Zhang, Z. L. Wang, Z. Li, *Adv. Funct. Mater.* **2019**, *29*, 1807560; c) K. Meng, J. Chen, X. Li, Y. Wu, W. Fan, Z. Zhou, Q. He, X. Wang, X. Fan, Y. Zhang, J. Yang, Z. L. Wang, *Adv. Funct. Mater.* **2018**, *29*, 1806388; d) M. Amit, L. Chukoskie, A. J. Skalsky, H. Garudadri, T. N. Ng, *Adv. Funct. Mater.* **2019**, *30*, 1905241; e) C. M. Boutry, L. Beker, Y. Kaizawa, C. Vassos, H. Tran, A. C. Hincley, R. Pfattner, S. Niu, J. Li, J. Claverie, Z. Wang, J. Chang, P. M. Fox, Z. Bao, *Nat. Biomed. Eng.* **2019**, *3*, 47.
- [6] a) H. Pan, G. Xie, W. Pang, S. Wang, Y. Wang, Z. Jiang, X. Du, H. Tai, *ACS Appl. Mater. Interfaces* **2020**, *12*, 38805. b) Y. Al-Handarish, O. M. Omisore, T. Igbe, S. Han, H. Li, W. Du, J. Zhang, L. Wang, *Adv. Mater. Sci. Eng.* **2020**, *2020*, 1; c) H. Ouyang, J. Tian, G. Sun, Y. Zou, Z. Liu, H. Li, L. Zhao, B. Shi, Y. Fan, Y. Fan, Z. L. Wang, Z. Li, *Adv. Mater.* **2017**, *29*, 1703456.
- [7] a) M. Irimia-Vladu, E. D. Glowacki, G. Voss, S. Bauer, N. S. Sariciftci, *Mater. Today* **2012**, *15*, 340; b) G. Zheng, X. Xu, B. Li, K. Wu, T. A. Yekeen, X. Huo, *J. Exposure Sci. Environ. Epidemiol.* **2013**, *23*, 67; c) B. Zhu, H. Wang, W. R. Leow, Y. Cai, X. J. Loh, M. Y. Han, X. Chen, *Adv. Mater.* **2016**, *28*, 4250; d) M. Jian, Y. Zhang, Z. Liu, *Chin. J. Polym. Sci.* **2020**, *38*, 459; e) M. Irimia-Vladu, *Chem. Soc. Rev.* **2014**, *43*, 588.
- [8] a) R. Schirhagl, C. Weder, J. Lei, C. Werner, H. M. Textor, *Chem. Soc. Rev.* **2016**, *45*, 234; b) B. Bhushan, Y. C. Jung, *Prog. Mater. Sci.* **2011**, *56*, 1; c) J. Hunt, B. Bhushan, *J. Colloid Interface Sci.* **2011**, *363*, 187.
- [9] a) S. Yu, L. Li, J. Wang, E. Liu, J. Zhao, F. Xu, Y. Cao, C. Lu, *Adv. Funct. Mater.* **2020**, *30*, 1907091; b) L. Csoka, I. C. Hoeger, O. J. Rojas, I. Peszlen, J. J. Pawlak, P. N. Peralta, *ACS Macro Lett.* **2012**, *1*, 867; c) Y. Liu, K. He, G. Chen, W. R. Leow, X. Chen, *Chem. Rev.* **2017**, *117*, 12893; d) B. Bhushan, *Philos. Trans. R. Soc., A* **2009**, *367*, 1445; e) L. Wang, D. Chen, K. Jiang, G. Shen, *Chem. Soc. Rev.* **2017**, *46*, 6764; f) Z. Li, Q. Zheng, Z. L. Wang, Z. Li, *Research* **2020**, *2020*, 8710686.
- [10] S. Kang, J. Lee, S. Lee, S. Kim, J.-K. Kim, H. Algadi, S. Al-Sayari, D.-E. Kim, D. Kim, T. Lee, *Adv. Electron. Mater.* **2016**, *2*, 1600356.
- [11] Q. Tian, W. Yan, Y. Li, D. Ho, *ACS Appl. Mater. Interfaces* **2020**, *12*, 9710.
- [12] a) H. Li, S. Lv, Y. Fang, *Nano Res.* **2020**, *13*, 1244; b) B. Bhushan, Y. C. Jung, *Nanotechnology* **2006**, *17*, 2758; c) G. Eglinton, R. J. Hamilton, *Science* **1967**, *156*, 1322.
- [13] T. Zhao, T. Li, L. Chen, L. Yuan, X. Li, J. Zhang, *ACS Appl. Mater. Interfaces* **2019**, *11*, 29466.
- [14] a) S. E. Naleway, M. M. Porter, J. McKittrick, M. A. Meyers, *Adv. Mater.* **2015**, *27*, 5455; b) Z. Ling, T. Wang, M. Makarem, M. Santiago Cintrón, H. N. Cheng, X. Kang, M. Bacher, A. Potthast, T. Rosenau, H. King, C. D. Delhom, S. Nam, J. Vincent Edwards, S. H. Kim, F. Xu, A. D. French, *Cellulose* **2019**, *26*, 305.
- [15] Y. Wei, S. Chen, Y. Lin, X. Yuan, L. Liu, *J. Mater. Chem. C* **2016**, *4*, 935.
- [16] G. Zhang, Q. Liao, Z. Zhang, Q. Liang, Y. Zhao, X. Zheng, Y. Zhang, *Adv. Sci.* **2016**, *3*, 1500257.
- [17] S. K. Karan, S. Maiti, O. Kwon, S. Paria, A. Maitra, S. K. Si, Y. Kim, J. K. Kim, B. B. Khatua, *Nano Energy* **2018**, *49*, 655.
- [18] S. Maiti, S. Kumar Karan, J. Lee, A. Kumar Mishra, B. Bhusan Khatua, J. Kon Kim, *Nano Energy* **2017**, *42*, 282.
- [19] Y. Wan, Z. Qiu, J. Huang, J. Yang, Q. Wang, P. Lu, J. Yang, J. Zhang, S. Huang, Z. Wu, C. F. Guo, *Small* **2018**, *14*, 1801657.
- [20] Y. Chen, Y. Jie, J. Wang, J. Ma, X. Jia, W. Dou, X. Cao, *Nano Energy* **2018**, *50*, 441.
- [21] Y. Jie, X. Jia, J. Zou, Y. Chen, N. Wang, Z. L. Wang, X. Cao, *Adv. Energy Mater.* **2018**, *8*, 1703133.
- [22] Q. Wang, M. Jian, C. Wang, Y. Zhang, *Adv. Funct. Mater.* **2017**, *27*, 1605657.
- [23] L. Li, T. Hu, H. Sun, J. Zhang, A. Wang, *ACS Appl. Mater. Interfaces* **2017**, *9*, 18001.
- [24] M. L. Hammock, A. Chortos, B. C. Tee, J. B. Tok, Z. Bao, *Adv. Mater.* **2013**, *25*, 5997.
- [25] a) B. Zhu, Z. Niu, H. Wang, W. R. Leow, H. Wang, Y. Li, L. Zheng, J. Wei, F. Huo, X. Chen, *Small* **2014**, *10*, 3625; b) C. L. Choong, M. B. Shim, B. S. Lee, S. Jeon, D. S. Ko, T. H. Kang, J. Bae, S. H. Lee, K. E. Byun, J. Im, Y. J. Jeong, C. E. Park, J. J. Park, U. I. Chung, *Adv. Mater.* **2014**, *26*, 3451; c) J. Park, Y. Lee, J. Hong, M. Ha, Y.-D. Jung, H. Lim, S. Y. Kim, H. Ko, *ACS Nano* **2014**, *8*, 4689; d) X. Xu, R. Wang, P. Nie, Y. Cheng, X. Lu, L. Shi, J. Sun, *ACS Appl. Mater. Interfaces* **2017**, *9*, 14273.
- [26] a) M. Kobayashi, T. Irisawa, B. Magyari-Kope, K. Saraswat, H. S. P. Wong, Y. Nishi, *IEEE Trans. Electron Devices* **2010**, *57*, 1037; b) Y. J. Park, B. K. Sharma, S. M. Shinde, M. S. Kim, B. Jang, J. H. Kim, J. H. Ahn, *ACS Nano* **2019**, *13*, 3023.
- [27] S. Jung, J. H. Kim, J. Kim, S. Choi, J. Lee, I. Park, T. Hyeon, D. H. Kim, *Adv. Mater.* **2014**, *26*, 4825.
- [28] a) W.-Y. Chang, T.-H. Fang, H.-J. Lin, Y.-T. Shen, Y.-C. Lin, *J. Disp. Technol.* **2009**, *5*, 178; b) F. V. Hatzivasiliou, S. G. Tzafesta, *J. Intell. Rob. Syst.* **1994**, *10*, 243.
- [29] J. G. Dabling, A. Filatov, W. W. Jason, *34th Annual International Conference of the IEEE EMBS, IEEE, Piscataway, NJ* **2012**, p. 162.
- [30] a) M. Wegener, W. Wirges, R. Gerhard-Multhaupt, *Adv. Eng. Mater.* **2005**, *7*, 1128; b) M. G. Broadhurst, G. T. Davis, *Ferroelectrics* **2011**, *60*, 3.
- [31] C. Pan, Z. Li, W. Guo, J. Zhu, Z. L. Wang, *Angew. Chem., Int. Ed. Engl.* **2011**, *50*, 11192.

- [32] a) T. Sharma, S.-S. Je, B. Gill, J. X. J. Zhang, *Sens. Actuators, A* **2012**, 177, 87; b) A. V. Shirinov, W. K. Schomburg, *Sens. Actuators, A* **2008**, 142, 48.
- [33] a) F.-R. Fan, Z.-Q. Tian, Z. Lin Wang, *Nano Energy* **2012**, 1, 328; b) B. A. Grzybowski, A. Winkleman, J. A. Wiles, Y. Brumer, G. M. Whitesides, *Nat. Mater.* **2003**, 2, 241.
- [34] S. Niu, Z. L. Wang, *Nano Energy* **2015**, 14, 161.
- [35] a) G. Zhu, C. Pan, W. Guo, C. Y. Chen, Y. Zhou, R. Yu, Z. L. Wang, *Nano Lett.* **2012**, 12, 4960; b) F. Yi, L. Lin, S. Niu, P. K. Yang, Z. Wang, J. Chen, Y. Zhou, Y. Zi, J. Wang, Q. Liao, Y. Zhang, Z. L. Wang, *Adv. Funct. Mater.* **2015**, 25, 3688; c) X. Qu, X. Ma, B. Shi, H. Li, L. Zheng, C. Wang, Z. Liu, Y. Fan, X. Chen, Z. Li, Z. L. Wang, *Adv. Funct. Mater.* **2020**, 31, 2006612.
- [36] W. Barthlott, C. Neinhuis, *Planta* **1997**, 202, 1.
- [37] a) H.-J. Jin, D. L. Kaplan, *Nature* **2003**, 424, 1057; b) P. Wagner, R. Furstner, W. Barthlott, C. Neinhuis, *J. Exp. Bot.* **2003**, 54, 1295.
- [38] a) B. Bhushan, *J. Adhes. Sci. Technol.* **2007**, 21, 1213; b) K. Autumn, Y. A. Liang, S. T. Hsieh, W. Zesch, W. P. Chan, T. W. Kenny, R. Fearing, R. J. Full, *Nature* **2000**, 405, 681.
- [39] B. Su, S. Gong, Z. Ma, L. W. Yap, W. Cheng, *Small* **2015**, 11, 1886.
- [40] a) M. Ha, S. Lim, S. Cho, Y. Lee, S. Na, C. Baig, H. Ko, *ACS Nano* **2018**, 12, 3964; b) C. M. Boutry, M. Negre, M. Jorda, O. Vardoulis, A. Chortos, O. Khatib, Z. Bao, *Sci. Rob.* **2018**, 3, eaau6914; c) M. Ha, S. Lim, J. Park, D.-S. Um, Y. Lee, H. Ko, *Adv. Funct. Mater.* **2015**, 25, 2841; d) X. Li, Y. J. Fan, H. Y. Li, J. W. Cao, Y. C. Xiao, Y. Wang, F. Liang, H. L. Wang, Y. Jiang, Z. L. Wang, G. Zhu, *ACS Nano* **2020**, 14, 9605.
- [41] Y. Guo, Z. Guo, M. Zhong, P. Wan, W. Zhang, L. Zhang, *Small* **2018**, 14, 1803018.
- [42] K. Wang, Z. Lou, L. Wang, L. Zhao, S. Zhao, D. Wang, W. Han, K. Jiang, G. Shen, *ACS Nano* **2019**, 13, 9139.
- [43] J. Yang, J. Chen, Y. Su, Q. Jing, Z. Li, F. Yi, X. Wen, Z. Wang, Z. L. Wang, *Adv. Mater.* **2015**, 27, 1316.
- [44] a) Y. Ding, T. Xu, O. Onyilagha, H. Fong, Z. Zhu, *ACS Appl. Mater. Interfaces* **2019**, 11, 6685; b) Y. Hosoyamada, T. Sakai, *Anat. Embryol.* **2005**, 210, 1.
- [45] a) C. Metzger, E. Fleisch, J. Meyer, M. Dansachmüller, I. Graz, M. Kaltenbrunner, C. Keplinger, R. Schwödiauer, S. Bauer, *Appl. Phys. Lett.* **2008**, 92, 013506; b) M. Shimojo, A. Namiki, M. Ishikawa, R. Makino, K. Mabuchi, *IEEE Sens. J.* **2004**, 4, 589; c) H.-K. Lee, S.-I. Chang, E. Yoon, *J. Microelectromech. Syst.* **2006**, 15, 1681.
- [46] a) F. Natalio, T. P. Corrales, M. Panthöfer, D. Schollmeyer, I. Lieberwirth, W. E. G. Müller, M. Kappl, H.-J. Butt, W. Tremel, *Science* **2013**, 339, 1298; b) G. Duan, S. Jiang, V. Jérôme, J. H. Wendorff, A. Fathi, J. Uhm, V. Altstädt, M. Herling, J. Breu, R. Freitag, S. Agarwal, A. Greiner, *Adv. Funct. Mater.* **2015**, 25, 2850.
- [47] S. C. Mannsfeld, B. C. Tee, R. M. Stoltenberg, C. V. Chen, S. Barman, B. V. Muir, A. N. Sokolov, C. Reese, Z. Bao, *Nat. Mater.* **2010**, 9, 859.
- [48] a) R. Xu, A. Zverev, A. Hung, C. Shen, L. Irie, G. Ding, M. Whitmeyer, L. Ren, B. Griffin, J. Melcher, L. Zheng, X. Zang, M. Sanghadasa, L. Lin, *Microsyst. Nanoeng.* **2018**, 4, 36; b) W. Sun, L. Wan, X. Li, X. Zhao, X. Yan, *J. Mater. Chem. A* **2016**, 4, 10948.
- [49] Y. Q. Liu, J. R. Zhang, D. D. Han, Y. L. Zhang, H. B. Sun, *ACS Appl. Mater. Interfaces* **2019**, 11, 38084.
- [50] Z. Qiu, Y. Wan, W. Zhou, J. Yang, J. Yang, J. Huang, J. Zhang, Q. Liu, S. Huang, N. Bai, Z. Wu, W. Hong, H. Wang, C. F. Guo, *Adv. Funct. Mater.* **2018**, 28, 1802343.
- [51] a) J. Shi, L. Wang, Z. Dai, L. Zhao, M. Du, H. Li, Y. Fang, *Small* **2018**, 14, 1800819; b) T. Li, H. Luo, L. Qin, X. Wang, Z. Xiong, H. Ding, Y. Gu, Z. Liu, T. Zhang, *Small* **2016**, 12, 5042.
- [52] R. Guo, Y. Yu, J. Zeng, X. Liu, X. Zhou, L. Niu, T. Gao, K. Li, Y. Yang, F. Zhou, Z. Zheng, *Adv. Sci.* **2015**, 2, 1400021.
- [53] P. Nie, R. Wang, X. Xu, Y. Cheng, X. Wang, L. Shi, J. Sun, *ACS Appl. Mater. Interfaces* **2017**, 9, 14911.
- [54] S. R. A. Ruth, V. R. Feig, H. Tran, Z. Bao, *Adv. Funct. Mater.* **2020**, 30, 2003491.
- [55] D. W. Bechert, M. Bruse, W. Hage, *Exp. Fluids* **2000**, 28, 403.
- [56] H. Gao, X. Wang, H. Yao, S. Gorb, E. Arzt, *Mech. Mater.* **2005**, 37, 275.
- [57] G. Nyström, A. Mhraryan, A. Razaq, T. Lindström, L. Nyholm, M. Strømme, *J. Phys. Chem. B* **2010**, 114, 4178.
- [58] X. Wang, O. Yue, X. Liu, M. Hou, M. Zheng, *Chem. Eng. J.* **2020**, 392, 123672.
- [59] a) M. Shoda, Y. Sugano, *Biotechnol. Bioprocess Eng.* **2005**, 10, 1; b) Y. Huang, C. Zhu, J. Yang, Y. Nie, C. Chen, D. Sun, *Cellulose* **2014**, 21, 1.
- [60] H. Zhu, W. Luo, P. N. Ciesielski, Z. Fang, J. Y. Zhu, G. Henriksson, M. E. Himmel, L. Hu, *Chem. Rev.* **2016**, 116, 9305.
- [61] S. K. Mahadeva, K. Walus, B. Stoeber, *ACS Appl. Mater. Interfaces* **2015**, 7, 8345.
- [62] M. D. Shoulders, R. T. Raines, *Annu. Rev. Biochem.* **2009**, 78, 929.
- [63] Y. Lin, D. Gritsenko, Q. Liu, X. Lu, J. Xu, *ACS Appl. Mater. Interfaces* **2016**, 8, 20501.
- [64] A. Russo, B. Y. Ahn, J. J. Adams, E. B. Duoss, J. T. Bernhard, J. A. Lewis, *Adv. Mater.* **2011**, 23, 3426.
- [65] L. Q. Tao, K. N. Zhang, H. Tian, Y. Liu, D. Y. Wang, Y. Q. Chen, Y. Yang, T. L. Ren, *ACS Nano* **2017**, 11, 8790.
- [66] a) K. N. Kim, J. Chun, S. A. Chae, C. W. Ahn, I. W. Kim, S.-W. Kim, Z. L. Wang, J. M. Baik, *Nano Energy* **2015**, 14, 87; b) C. K. Jeong, I. Kim, K.-I. Park, M. H. Oh, H. Paik, G.-T. Hwang, K. No, Y. S. Nam, K. J. Lee, *ACS Nano* **2013**, 7, 11016.
- [67] a) N. Huebsch, D. J. Mooney, *Nature* **2009**, 462, 426; b) B. Scholz, G. Liebezeit, *J. Appl. Physiol.* **2012**, 25, 643.
- [68] a) E. Fukada, *J. Phys. Soc. Jpn.* **1955**, 10, 149; b) M. Askari, A. R. Saidi, A. S. Rezaei, *Compos. Struct.* **2017**, 179, 340.
- [69] E. Fukada, *J. Phys. Soc. Jpn.* **1957**, 12, 1158.
- [70] V. R. Binetti, J. D. Schiffman, O. D. Leaffer, J. E. Spanier, C. L. Schauer, *Integr. Biol.* **2009**, 1, 324.
- [71] a) G. Eglinton, A. G. Gonzalez, R. J. Haiilton, R. A. Raphael, *Phytocystmistry* **1962**, 1, 89; b) Z. Guo, W. Liu, *Plant Sci.* **2007**, 172, 1103.
- [72] a) U. G. Wegst, H. Bai, E. Saiz, A. P. Tomsia, R. O. Ritchie, *Nat. Mater.* **2015**, 14, 23; b) F. Barthelat, H. Tang, P. Zavattieri, C. Li, H. Espinosa, *J. Mech. Phys. Solids* **2007**, 55, 306.
- [73] a) L. Zhou, P. Fu, D. Wen, Y. Yuan, S. Zhou, *Appl. Catal., B* **2016**, 181, 635; b) L. Deng, H. Yuan, X. Cai, Y. Ruan, S. Zhou, Y. Chen, Y. Yuan, *Int. J. Hydrogen Energy* **2016**, 41, 22328.
- [74] a) T. Yucel, P. Cebe, D. L. Kaplan, *Adv. Funct. Mater.* **2011**, 21, 779; b) J. A. Kluge, O. Rabotyagova, G. G. Leisk, D. L. Kaplan, *Trends Biotechnol.* **2008**, 26, 244.
- [75] N. Du, Z. Yang, X. Y. Liu, Y. Li, H. Y. Xu, *Adv. Funct. Mater.* **2011**, 21, 772.
- [76] E. Fukada, *Wood Sci. Technol.* **1968**, 2, 299;
- [77] S. Rajala, T. Siponkoski, E. Sarlin, M. Mettanan, M. Vuoriluoto, A. Pammo, J. Juuti, O. J. Rojas, S. Franssila, S. Tuukkanen, *ACS Appl. Mater. Interfaces* **2016**, 8, 15607.
- [78] a) M. Giese, M. K. Khan, W. Y. Hamad, M. J. MacLachlan, *ACS Macro Lett.* **2013**, 2, 818; b) L. Persano, C. Dagdeviren, C. Maruccio, L. De Lorenzis, D. Pisignano, *Adv. Mater.* **2014**, 26, 7574.
- [79] A. Goldbourt, *Prog. Nucl. Magn. Reson. Spectrosc.* **2019**, 114–115, 192.
- [80] a) B. Y. Lee, J. Zhang, C. Zueger, W. J. Chung, S. Y. Yoo, E. Wang, J. Meyer, R. Ramesh, S. W. Lee, *Nat. Nanotechnol.* **2012**, 7, 351; b) I. W. Park, K. W. Kim, Y. Hong, H. J. Yoon, Y. Lee, D. Gwak, K. Heo, *Nanomaterials* **2020**, 10, 93.
- [81] S. K. Ghosh, D. Mandal, *Appl. Phys. Lett.* **2016**, 109, 103701.
- [82] S. K. Ghosh, D. Mandal, *ACS Sustainable Chem. Eng.* **2017**, 5, 8836.
- [83] S. K. Ghosh, D. Mandal, *Nano Energy* **2016**, 28, 356.

- [84] N. A. Hoque, P. Thakur, P. Biswas, M. M. Saikh, S. Roy, B. Bagchi, S. Das, P. P. Ray, *J. Mater. Chem. A* **2018**, *6*, 13848.
- [85] A. A. Marino, B. D. Gross, *Arch. Oral Biol.* **1989**, *34*, 507.
- [86] S. K. Karan, S. Maiti, S. Paria, A. Maitra, S. K. Si, J. K. Kim, B. B. Khatua, *Mater. Today Energy* **2018**, *9*, 114.
- [87] S. K. Ghosh, D. Mandal, *Appl. Phys. Lett.* **2017**, *110*, 123701.
- [88] N. R. Alluri, N. P. Maria Joseph Raj, G. Khandelwal, V. Vivekananthan, S.-J. Kim, *Nano Energy* **2020**, *73*, 104767.
- [89] A. Gaur, S. Tiwari, C. Kumar, P. Maiti, *Energy Rep.* **2020**, *6*, 490.
- [90] S. Bairagi, S. Ghosh, S. W. Ali, *Sci. Rep.* **2020**, *10*, 12121.
- [91] D.-M. Shin, H. J. Han, W.-G. Kim, E. Kim, C. Kim, S. W. Hong, H. K. Kim, J.-W. Oh, Y.-H. Hwang, *Energy Environ. Sci.* **2015**, *8*, 3198.
- [92] a) V. Slabov, S. Kopyl, M. P. Soares dos Santos, A. L. Kholkin, *Nano-Micro Lett.* **2020**, *12*, 41; b) S. Maiti, S. K. Karan, J. K. Kim, B. B. Khatua, *Adv. Energy Mater.* **2019**, *9*, 1803027; c) D. Jiang, B. Shi, H. Ouyang, Y. Fan, Z. L. Wang, Z. Li, *ACS Nano* **2020**, *14*, 6436.
- [93] a) J.-G. Sun, T.-N. Yang, C.-Y. Wang, L.-J. Chen, *Nano Energy* **2018**, *48*, 383; b) G. Zhao, Y. Zhang, N. Shi, Z. Liu, X. Zhang, M. Wu, C. Pan, H. Liu, L. Li, Z. L. Wang, *Nano Energy* **2019**, *59*, 302; c) B. D. Chen, W. Tang, C. Zhang, L. Xu, L. P. Zhu, L. J. Yang, C. He, J. Chen, L. Liu, T. Zhou, Z. L. Wang, *Nano Res.* **2018**, *11*, 3096.
- [94] a) M. L. Seol, J. H. Woo, D. I. Lee, H. Im, J. Hur, Y. K. Choi, *Small* **2014**, *10*, 3887; b) E.-L. Tan, M. G. Potroz, G. Ferracci, J. A. Jackman, H. Jung, L. Wang, N.-J. Cho, *Adv. Funct. Mater.* **2018**, *28*, 1707568.
- [95] H.-J. Kim, E.-C. Yim, J.-H. Kim, S.-J. Kim, J.-Y. Park, I.-K. Oh, *Nano Energy* **2017**, *33*, 130.
- [96] a) L. Feng, Y. Zhang, J. Xi, Y. Zhu, N. Wang, F. Xia, L. Jiang, *Langmuir* **2008**, *24*, 4114; b) C. D. Holder, *J. Hydrol.* **2007**, *336*, 147.
- [97] Y. Feng, L. Zhang, Y. Zheng, D. Wang, F. Zhou, W. Liu, *Nano Energy* **2019**, *55*, 260.
- [98] H.-J. Kim, J.-H. Kim, K.-W. Jun, J.-H. Kim, W.-C. Seung, O. H. Kwon, J.-Y. Park, S.-W. Kim, I.-K. Oh, *Adv. Energy Mater.* **2016**, *6*, 1502329.
- [99] M. Martinez-Sanz, F. Pettolino, B. Flanagan, M. J. Gidley, E. P. Gilbert, *Carbohydr. Polym.* **2017**, *175*, 450.
- [100] M. Wang, R. Li, X. Feng, C. Dang, F. Dai, X. Yin, M. He, D. Liu, H. Qi, *ACS Appl. Mater. Interfaces* **2020**, *12*, 27545.
- [101] Z. Chen, H. Zhuo, Y. Hu, H. Lai, L. Liu, L. Zhong, X. Peng, *Adv. Funct. Mater.* **2020**, *30*, 1910292.
- [102] L. Wang, J. A. Jackman, E.-L. Tan, J. H. Park, M. G. Potroz, E. T. Hwang, N.-J. Cho, *Nano Energy* **2017**, *36*, 38.
- [103] D. Wang, L. Wang, Z. Lou, Y. Zheng, K. Wang, L. Zhao, W. Han, K. Jiang, G. Shen, *Nano Energy* **2020**, *78*, 105252.
- [104] a) Y. Chen, L. Hu, C. Li, B. Dang, Q. Sun, T. Zhai, H. Li, *InfoMat* **2020**, *2*, 1225; b) Y. Li, Y. A. Samad, K. Liao, *J. Mater. Chem. A* **2015**, *3*, 2181.
- [105] a) S. Wang, Z. Ren, J. Li, Y. Ren, L. Zhao, J. Yu, *RSC Adv.* **2014**, *4*, 31300; b) M. Li, Y. Xiong, X. Liu, C. Han, Y. Zhang, X. Bo, L. Guo, *J. Mater. Chem. A* **2015**, *3*, 9658.
- [106] J. Yang, Y. Li, Y. Zheng, Y. Xu, Z. Zheng, X. Chen, W. Liu, *Small* **2019**, *15*, 1902826.
- [107] X. Zheng, H. Lee, T. H. Weisgraber, M. Shusteff, J. Duoss, E. B. Duoss, J. D. Kuntz, M. M. Biener, Q. Ge, J. A. Jackson, S. O. Kucheyev, N. X. Fang, C. M. Spadaccini, *Science* **2014**, *344*, 1373.
- [108] A. Elsayes, V. Sharma, K. Yiannacou, A. Koivikko, A. Rasheed, V. Sariola, *Adv. Sustainable Syst.* **2020**, *4*, 2000056.



**Hong Pan** is a doctoral candidate in the School of Optoelectronic Science and Engineering at University of Electronic Science and Technology of China (UESTC). In 2019, she joined the Department of Materials Science and Engineering at Seoul National University as a visiting Ph.D. Student under the supervision of Prof. Tae-Woo Lee. Her current research interests include gas sensors and wearable pressure sensors.



**Tae-Woo Lee** is a full professor in materials science and engineering at the Seoul National University, Korea. He joined Bell Laboratories, USA, as a postdoctoral researcher and then worked at Samsung Advanced Institute of Technology as a senior member of research staff (2003–2008). He was an associate professor in materials science and engineering at the Pohang University of Science and Technology (POSTECH), Korea until August 2016. He has been a Materials Research Society (MRS) Fellow since 2020. His research focuses on flexible or printed electronics based on organic and organic–inorganic hybrid materials for displays, solid-state lighting and neuromorphic bioelectronics.